

Summer 2024

Geoelectrical And Hydrochemical Characterization of Submarine Groundwater Discharge in Florida Bay

Ifeanyi Emmanuel Eze

Follow this and additional works at: <https://digitalcommons.georgiasouthern.edu/etd>



Part of the [Environmental Monitoring Commons](#), [Fresh Water Studies Commons](#), [Geochemistry Commons](#), [Geology Commons](#), and the [Hydrology Commons](#)

Recommended Citation

Eze, Ifeanyi Emmanuel, "Geoelectrical And Hydrochemical Characterization of Submarine Groundwater Discharge in Florida Bay" (2024). *Electronic Theses and Dissertations*. 2827. <https://digitalcommons.georgiasouthern.edu/etd/2827>

This thesis (open access) is brought to you for free and open access by the Jack N. Averitt College of Graduate Studies at Georgia Southern Commons. It has been accepted for inclusion in Electronic Theses and Dissertations by an authorized administrator of Georgia Southern Commons. For more information, please contact digitalcommons@georgiasouthern.edu.

GEOELECTRICAL AND HYDROCHEMICAL CHARACTERIZATION OF SUBMARINE
GROUNDWATER DISCHARGE IN FLORIDA BAY

by

IFEANYI EZE

(Under the direction of Jacque Kelly)

ABSTRACT

Florida Bay, situated at the southern tip of Everglades National Park and underlain by the Miami Limestone formation, is an ecosystem of global significance. Over the past century, the bay has faced threats such as droughts, seagrass mortality, and hypersalinity. Despite various studies and management efforts, the dynamics of submarine groundwater discharge (SGD) in the region remain underexplored. Given that SGD plays a significant role in the chemical dynamics of coastal ecosystems, it warrants thorough investigation. This study aims to characterize the spatial and temporal patterns of SGD in Florida Bay by surveying three basins – Rankin, Whipray, and Rabbit Key – from 2021 to 2024, covering both wet and dry seasons. Using electrical resistivity tomography (ERT) with a dipole-dipole array, I mapped marine resistivity, revealing low bulk resistivity values (0.1 - 4.0 Ωm) across the study area. Elevated resistivity anomalies upwelling from the limestone units were interpreted as possible SGD zones, prompting in-situ radon-222 and salinity measurements for validation. The hypersaline nature of groundwater, with concentrations up to 45 ppt in Rankin Basin, indicates the SGD is recirculated seawater. The identification of pockets of saline SGD and no fresh SGD underscored the difficulty in using ERT method in areas of minimal salinity variations and low resistivity ranges with respect to groundwater. I postulate that the geophysical anomalies primarily stem from subsurface petrophysical properties rather than

groundwater chemistry. This study enriches our understanding of Florida Bay's hydrology and informs future scientific research and management efforts.

INDEX WORDS: Florida Bay, Electrical resistivity tomography, Submarine groundwater discharge, Salinity, Seagrass, Groundwater, Radon, Rankin Basin, Whipray Basin, Rabbit Key Basin

GEOELECTRICAL AND HYDROCHEMICAL CHARACTERIZATION OF SUBMARINE
GROUNDWATER DISCHARGE IN FLORIDA BAY

by

IFEANYI EMMANUEL EZE

B.Sc., Nnamdi Azikiwe University, Nigeria, 2018

A Thesis Submitted to the Graduate Faculty of Georgia Southern University in Partial
Fulfillment of the Requirements for the Degree

MASTER OF SCIENCE IN APPLIED GEOGRAPHY

STATESBORO, GEORGIA

© 2024

IFEANYI EZE

All Rights Reserved

GEOELECTRICAL AND HYDROCHEMICAL CHARACTERIZATION OF SUBMARINE
GROUNDWATER DISCHARGE IN FLORIDA BAY

by

IFEANYI EZE

Major Professor: Jacqué J. Kelly
Committee: Munshi K. Rahman
John M. Carroll

Electronic Version Approved:
July 2024

DEDICATION

To my mother, Roseline Anenechukwu Maduadichie, who would sacrifice any comfort to ensure my well-being. I wish we could discuss and cheer on each field trip, data analysis, and corrections that went into this thesis. Unfortunately, nature had other plans. Rest in peace, Mom

ACKNOWLEDGEMENTS

I am profoundly grateful to everyone who contributed to the successful completion of this research project. I extend my heartfelt thanks to my undergraduate advisor, Dr. Charity Nwokeabia, and the faculty members of the Geological Sciences Department at Nnamdi Azikiwe University, Nigeria, for providing me with a solid foundation in geosciences. I am also grateful to the Geosciences program at Georgia Southern University for the opportunity to conduct this research.

I am deeply indebted to Professor Jacque Kelly, my academic advisor. You have been the guiding angel that God used to reignite my passion for science. Thank you for taking a chance on me. This work would not have been possible without your expert knowledge, support and encouragement. I also wish to thank Dr. John Carroll and Dr. Munshi Rahman for serving on my committee and for their invaluable mentorship. Special thanks to Dr. Christine Hladik for her guidance on statistical analysis and for pointing me in the right direction. My sincere regards go to Dr. Brad Furman and the entire field crew who assisted in data collection in Florida Bay.

Lastly, I would like to thank my family and friends in Nigeria for their unwavering support and belief in me. Your encouragement is truly inspiring. To everyone who contributed to my success, directly or indirectly, I am deeply grateful. Thank you.

TABLE OF CONTENTS

DEDICATION 2

ACKNOWLEDGEMENTS 3

CHAPTER

1 INTRODUCTION 6

 Background of Study 6

 Overview of Submarine Groundwater Discharge 8

 Overview of Techniques for Mapping Submarine Groundwater Discharge 9

 Description of the Study Area..... 12

 Geology of Florida Bay 13

 Ecology of Florida Bay and Seagrass Die-off 15

 Climate Action in Florida Bay 17

 Management Efforts in Florida Bay 18

 Survey Site Selection 19

 Previous SGD Studies in Florida Bay 20

 Research Questions and Overview of Thesis..... 22

2 MATERIALS AND METHODS24

 Electrical Resistivity as a Field Data Acquisition Technique in Florida Bay..... 24

 Electrical Resistivity Method Background 24

 Electrical Resistivity Profile Collection..... 25

 Ground Truth Data Collection 29

3 DATA PROCESSING, ANALYSIS, AND RESULTS32

 Electrical Resistivity Profile Processing 32

 Results of Electrical Resistivity Profiles..... 35

 Geospatial Analysis of Groundwater Sample Locations 37

 Radon Data Processing 38

 Results of Groundwater Data..... 39

 Statistical Analysis of Groundwater Samples 40

4 INTERPRETATION OF RESULTS AND DISCUSSION43

 Electrical Resistivity Profiles..... 43

 Statistical Interpretation of Groundwater Samples 49

 Groundwater End Members 51

	5
Broader Implications.....	54
Limitations and Future Steps	56
Conclusion	57
REFERENCES	59
APPENDICES	80

CHAPTER 1

INTRODUCTION

1.1 Background of Study

Coastal ecosystems, encompassing areas from 50 meters below mean sea level to 50 meters above high tide and extending 100 kilometers inland from the shore, occupy about 4% of the Earth's landmass and 11% of the oceanic regions (Lopez-Rivas & Cardenas, 2024). These environments are critical for biodiversity, providing habitats and breeding ground including seagrass beds, mangrove forests, and coral reefs (Fredley et al., 2019). However, coastal ecosystems are under threat, with many areas designated for conservation due to declining habitats (Fourqurean & Robble, 1999; Fredley et al., 2019). The proximity to human populations makes these environments highly susceptible to natural and anthropogenic impacts such as sea-level rise, pollution, habitat destruction, and climate change (Dessu et al., 2018; Fu et al., 2020). By 2050, coastal areas are projected to be home to 2.4 billion people worldwide (Zamrsky et al., 2024), and currently, over 40% of the US population resides in coastal counties (National Oceanic and Atmospheric Administration, 2024). These coastal areas are likely to experience significant changes due to the interaction of increasing populations, extreme weather events, climate change, and human activities.

Florida Bay, located at the southern tip of the Everglades National Park, is a critical example of such a shallow marine environment that has faced harsh ecological alterations. Due to water management practices, the natural flow of water in the Everglades, from the Kissimmee River to Lake Okeechobee and then to Florida Bay, has been disrupted by manmade levees and barriers (Stabenau & Kotun, 2012). This has resulted in an unbalanced water flow and insufficient freshwater reaching the environment (Fredley et al., 2019). Since the past century, the estuary has

suffered diverse threats including droughts, seagrass mortality, and hypersalinity (Fourqurean & Robble, 1999; Fredley et al., 2019; Robbins, 2023).

The factors driving alterations of natural habitats in this region have been widely debated. Prominent factors include seasonal hypersalinity (Fourqurean & Robblee, 1999), anthropogenic nutrient enrichment (Lapointe et al., 2004), and extreme temperature variations (Carlson et al., 2018). However, the impact of subterranean groundwater flows on the bay's hydrology and ecosystem remains largely unknown. This research aims to characterize submarine groundwater discharge (SGD) in the bay and investigate its physicochemical characteristics. Future extensions of the project could include assessing potential impacts of SGD on the bay's hydrological budget and ecosystem.

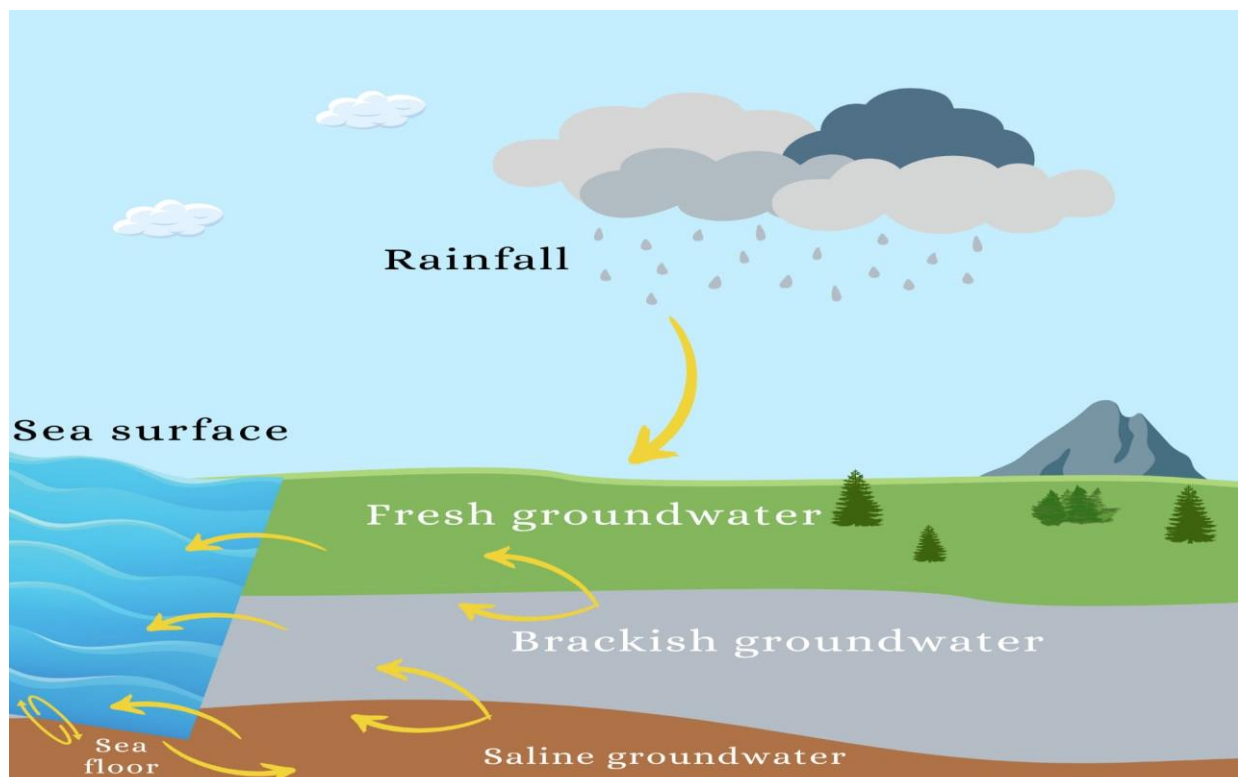


Fig. 1.1: Schematic of the key pathways for submarine groundwater discharge into the coast including the release of fresh groundwater and the recirculation of seawater through saline groundwater discharge.

1.2 Overview of Submarine Groundwater Discharge

The hydrological processes occurring within the seafloor are a complex array of phenomena with profound effects on marine dynamics. From the infiltration of freshwater into submerged aquifers to sediment transport along the seafloor and release of heated fluids from hydrothermal vents, these processes are interconnected and dynamic. Among these processes, SGD is especially important, serving as the key driver of interactions within marine ecosystems. SGD is any flow of water in the continental margin from the seabeds to the ocean, irrespective of the fluid composition or driving force (Burnett & Dulaiova, 2003; Moore, 2010). SGD may be a mixture of recirculated saline SGD and fresh SGD (Fig. 1.1; Taniguchi et al., 2002). While saline SGD is ubiquitous in coastal waters worldwide, the volume of fresh SGD is relatively small accounting for about 1% of total freshwater inputs to the coasts and less than 1% of total SGD (Santos et al., 2021). Fresh SGD acts as a localized point-source of new nutrients while saline SGD releases primarily recycled nutrients (Oehler et al., 2019), generated from degraded sediment organic matter, as well as from external nutrient sources brought in through the mixing of fresh and saline waters (Santos et al., 2021; Wilson, 2005). This complex subterranean flow of water is an important component of the hydrologic cycle and performs several ecological services such as nutrient cycling (Null et al., 2012), regulation of sea temperature and salinity (Juster et al., 1997), shifts in primary producer diversity (Kamermans et al., 2002) and removal of toxins (Burnett & Dulaiova, 2003). The factors that propel SGD include the terrestrial hydraulic gradient, variations in water level at permeable barriers, wave formation, tides, pressure gradients caused by storms or currents, convection, movement of the freshwater–seawater interface throughout the year, bioturbation, and geothermal heating (Burnett et al., 2006; Michael et al., 2005; Santos et al., 2021; Taniguchi et al., 2019). SGD manifests as diffuse seepage (often saline) or submarine springs

(often fresh) and can occur anywhere aquifers crop out in the marine environment at varying depths and distances from land (Santos et al., 2021; Taniguchi et al., 2019).

Although SGD occurs over a large spatial scale, it can transport a significant quantity of dissolved nutrients into the sea (Oehler et al., 2019; Wu et al., 2021). Several studies have shown that SGD serves as a conduit for nutrients and contaminants, which can have significant impacts on benthic ecosystems (e.g. Adyasari et al., 2020; Black et al., 2009; Burnett et al., 2003; Carlson et al., 2018; Kamermans et al., 2002; Kelly et al., 2018). The laden materials in groundwater can react with the coastal sediments and macrophytes including seagrasses and coral reefs (Kamermans et al., 2002; Oehler et al., 2019). Szymczycha et al. (2014) also found that SGD plays important roles in carbon transport in coastal ecosystems, hence influencing climate change. Pharmaceuticals can also be transported by SGD into the coastal ecosystem (Branchet et al., 2021).

Interest in SGD heightened in the twilight of the 20th century with a growing interest to characterize life underwater and understand seafloor processes in the face of climate change (Taniguchi et al., 2019). With United Nations' effort to preserve life below water, recent studies on coastal hydrology have focused on subterranean flow and its impacts on complex benthic ecosystems (Rocha et al., 2022). SGD is critical as coastal communities are becoming homes to teeming populations in the coastal environment.

1.3 Overview of Techniques for Mapping Submarine Groundwater Discharge

Various techniques have been used to locate and estimate specific fluxes of SGD. For example, various researchers have used scuba diving (Kamernans et al., 2002), remote sensing (Kelly et al., 2013; Samani et al., 2021; Tamborski et al., 2015), underwater spectroscopy (Eleftheriou et al., 2020), and isotope tracing (Adyasari et al., 2021; Burnett & Dulaiova, 2003; Cardenas et al., 2010). Wilson and Rocha (2012) proposed the application of Landsat ETM+ thermal infrared band in SGD studies. In a study carried out in Ireland, Wilson and Rocha (2012)

delineated the spatial distribution of SGD using the temperature anomaly plume estimation. In the Persian Gulf, the Landsat 8 thermal sensor was successfully used to delineate SGD at the coastlines (Jou-Claus et al., 2021; Samani et al., 2021). Kelly et al. (2013) employed aerial thermography to identify and quantify SGD in the Hawaiian Islands. Recent works on remote sensing of SGD involve the integration of multiple datasets and machine learning techniques (Gerlach et al., 2021).

Radium isotopes have been widely used to map SGD. They are vital tools for studying marine environments because they stay unchanged in seawater, decay predictably, and come from interactions between water and rocks or sediment (Garcia-Orellana et al., 2021; Zhang et al., 2017). In the northeastern Gulf of Mexico, Adyasari et al. (2021) detected storm-driven SGD using radium tracing methods. Moore (2003) established that the radioactive decay properties of radium-226 and radium-228 aid in accurately measuring groundwater flows and the decay rate provides a natural clock for estimating the age of water in subsurface environments. In Tampa Bay, Florida, Swarzenski et al. (2007a) integrated radium and radon measurements to delineate and quantify SGD along with its associated constituents. This was subsequently replicated by Zhang et al. (2017) in tracing SGD dynamics in Jiaozhou Bay, China.

Radon tracing is an alternative exploration technique that has proven effective in mapping SGD (e.g. Burnett & Dulaiova, 2003). This method leverages the radioactive decay of radon to trace the movement of groundwater from terrestrial sources into coastal and marine environments. Radon-222 has been widely acknowledged as a reliable natural indicator of SGD (Kelly et al., 2018). Ehlert Von Ahn et al. (2024) quantified the SGD by measuring the concentration of radon-222 in the coastal bay of the southern Baltic Sea. The utilization of radon tracing offers a non-invasive and cost-effective approach to studying SGD. Swarzenski and Izbicki (2009) employed a multi-method approach, integrating radium, radon, electromagnetic, and electrical techniques, to characterize SGD dynamics in the meso-tidal coastal waters adjacent to Santa Barbara Harbor,

California. Radon activity can be obtained from in-situ measurements (e.g. Kelly et al., 2018) for a more detailed characterization of SGD dynamics. This method can be used to validate other methods, thus providing a holistic understanding of groundwater-seawater interactions (Kelly et al., 2018).

Geophysical surveys are optimal tools for investigating SGD in complex estuary zones. Electromagnetic imaging (Attias et al., 2021), continuous electrical resistivity profiling (Cardenas et al., 2010; Stieglitz et al., 2008) and electrical resistivity tomography (Fu et al., 2020) have been used for SGD characterization. These techniques offer non-destructive probing and continuous monitoring and provide high-resolution data crucial for understanding SGD processes. Paepen et al. (2020) combined frequency-domain electromagnetic methods and electrical resistivity to map SGD at a littoral zone in the Belgian-French border. Electrical resistivity tomography (ERT) is one of the most established techniques for geophysical investigations. It is well suited for SGD studies due to its sensitivity to marine electrical conductivity (Fu et al, 2020; Hermans & Paepen, 2020). Cardenas et al. (2010) combined ERT and radon tracing to map regional sources of SGD in the Philippines. Fu et al. (2020) assessed the dynamics of SGD in the intertidal zone of Laizhou Bay, China using ERT. These studies have shown that ERT is an effective method for mapping SGD.

In this study, I will focus on the complementary techniques of ERT and radon measurements. Radon effectively delineates zones of SGD and classifies them into high and low areas of groundwater discharge (Kelly et al., 2018), while ERT provides detailed salinity profiles and compositional characteristics, distinguishing between freshwater and saltwater in the groundwater system (Dimova et al., 2012). Both techniques are non-invasive, making them ideal for non-destructive sampling in the National Park. ERT and radon tracing map subsurface processes and features and offer near-real-time measurements of SGD characteristics (Swarzenski et al., 2009).

1.4 Description of the Study Area

Florida Bay (Fig. 1.2) is a vast (2,200 square km), shallow (mean depth <2 m) triangular estuary located in the southern terminus of Everglades National Park, between the Florida Keys and the mainland Florida, United States (Corbett et al., 1999; Lee et al., 2006). To the west, a relatively open connection with the southwest Florida shelf facilitates the exchange of significant physical forcing, such as wind and tidal movements, into Florida Bay (Kelble et al., 2007; Yates & Halley, 2006). To the east, the Florida Keys, a Pleistocene reef, creates a limited exchange of water between the Atlantic Ocean and the bay (Kelble et al., 2007). The bay has extensive networks of submerged, anastomosing carbonate mudbanks which were compartmentalized into basins, covering nearly 30% of the bay (Carlson et al., 2018; Fourqurean & Robblee, 1999; Fredley et al., 2019; Juster et al., 1997). The mud banks influence water circulation patterns, surface water

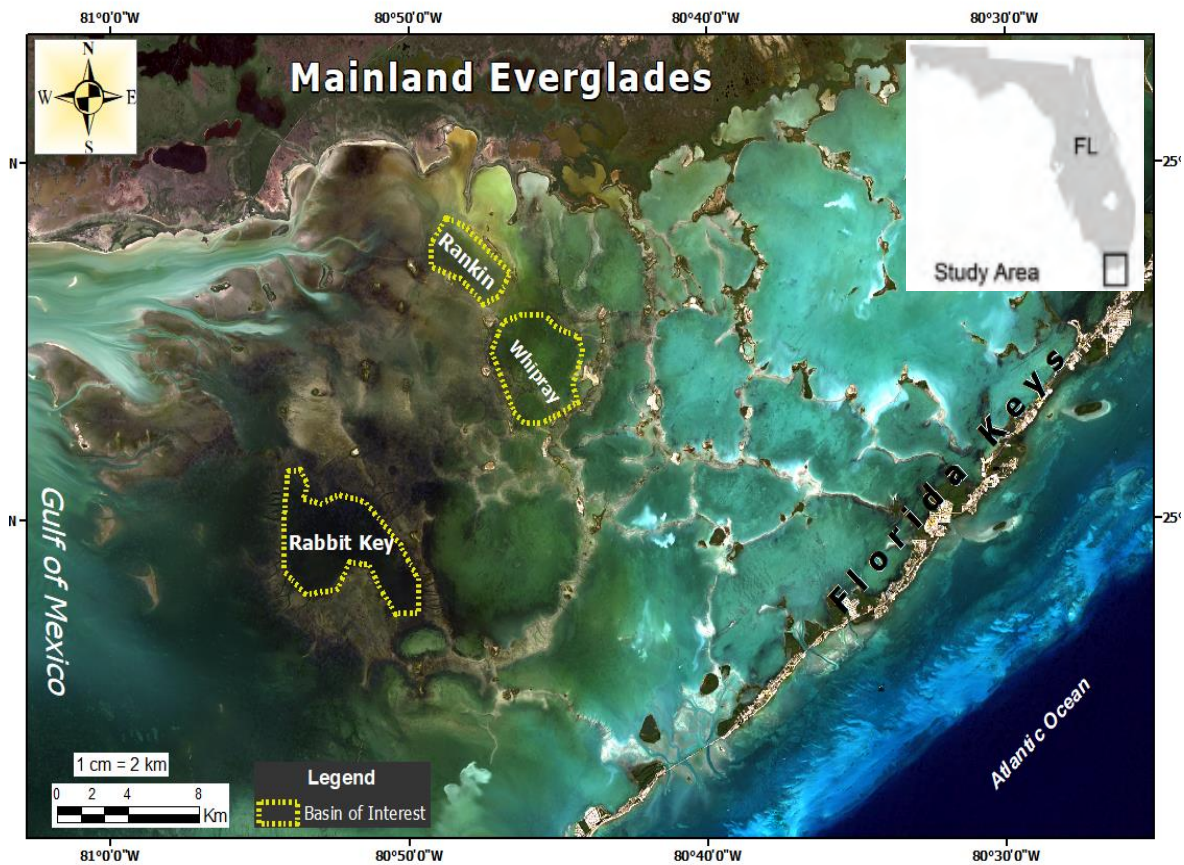


Fig 1.2: Map of the study area (Landsat OLI Imagery).

chemistry and distribution of benthic habitats (Yates & Halley, 2006). Systematic differences exist in the widths and depths of mud banks, and the sizes of their associated basins (Yates & Halley, 2006). Due to topographical differences and microtidal nature of the bay, the water level is several centimeters higher than the water level in the Atlantic Ocean (Reich et al., 2002). The depth of the water column typically ranges from 50 cm near the basin edges to 2 – 3 m in the channels and sections of the middle basins (Shank et al., 2011). Water residence times can be several months during the dry period in spring and early summer (Boyer et al., 1999; Shank et al., 2011). The environment has a tropical to subtropical climate with two distinct seasons (Juster et al., 1997). The wet season typically spans June through October and, on average, delivers 19.8 cm of rainfall while the dry season lasts from November to May and delivers 6.7 cm of rainfall, on average (National Oceanographic and Atmospheric Administration, 2022; Shank et al., 2011; Williams et al., 2009). The median water temperature across the Bay averages around 26°C and exhibits noticeable seasonal variations. Temperatures peak at approximately 30°C during the summer months and decrease to around 20°C during the winter months (Yates & Halley, 2006). The sustained higher temperature, elevated evaporation and low precipitation result in prolonged droughts in the bay (Carlson et al., 2018). Precipitation, evaporation, and water exchanges between basins and the coastal ocean all influence the salinity of Florida Bay (Stabenau & Kotun, 2012). Kelble et al. (2007) classified Florida Bay as seasonally hypersaline estuary, where hypersaline conditions prevail in early summer at the end of the dry season, and estuarine conditions (with salinity lower than the surrounding ocean) prevail in early winter at the end of the wet season.

1.4.1 Geology of Florida Bay

Florida Bay is within the Atlantic Coastal Plain of the eastern United States, which formed as a combination of depositional and erosional processes; characteristic of the late Pleistocene eustatic variations (Wanless & Tagett, 1989). It is within the Florida Key province of southern

Florida geology, consisting of oolitic limestone and a supratidal carbonate flat with several mangrove-fringed embayments and discontinuous low, shelly beach ridges (Enos & Perkins, 1979; Halley et al., 2004). The sediment mainly consists of biogenic aragonite (50–60%) and high-Mg calcite (30–40%), primarily produced by calcareous algae through in situ precipitation (Boyer et al., 1999; Jensen et al., 2009; Scott et al., 1997).

Sediments within the bay are deposited disconformably upon a nearly flat surface composed of pelletoidal Miami Limestone (Scott et al., 1997), which formed during the late Pleistocene when sea level was approximately 6 - 8 meters higher than today (Fourqurean & Robble, 1999; Halley et al., 2004). In outcropping regions, the oolitic facies exhibits cross bedding, reflecting the interaction of water currents on the ooids. These facies are like the marine environments of the Bahamas, where water currents circulate hypersaline water across the shoal (Purkis and Harris, 2017). The Bahamas ooids shoals are modern analogs of the Miami Limestone, offering insights into the sedimentological processes shaping Florida Bay.

The Miami Limestone covers the southern extent of the Biscayne aquifer system, a vital freshwater source for the metropolitan areas of South Florida (Halley et al., 2004). This aquifer system is unconfined and resides at relatively shallow depths, typically spanning from just a few meters to around 66 m deep, extending across the Miami Limestone formation (Cunningham & Florea, 2009; Halley et al., 2004). The fresh waters of the Biscayne aquifer discharge into coastal areas including Florida Bay (Cunningham & Florea, 2009). Owing to the karst system of the Miami Limestone (Halley et al., 2004), the limestone cavities are hydrological pathways for water to flow from the Biscayne aquifer to coastal ecosystems. Freshwater inputs from the Biscayne aquifer to the bay may occur, however, their discharge location and volumes have not been established. Cunningham and Florea (2009) documented areally extensive vuggy pores that serve as contaminant pathways and conduits for groundwater flow through the Biscayne aquifer. Below the

highly permeable Biscayne aquifer lies the deep-seated Floridan Aquifer, which is confined 250 - 300 m below Florida Bay (Fish & Stewart, 1991; Swarzenski et al., 2009).

1.4.2 Ecology of Florida Bay and Seagrass Die-off

Florida Bay, which is largely located within Everglades National Park, is a coastal system that provides habitat for diverse faunas and floras, and ecological support to the Florida Keys (Fredley et al., 2019; Zieman et al., 1999). The bay is characterized by extensive seagrass beds, particularly dominated by *Thalassia testudinum* (turtle grass), covering approximately 95% (1660 square km) of the seabeds (Zieman et al., 1989). These seagrass communities provide critical habitats for a plethora of marine species, including fish, crustaceans, and marine mammals, forming the foundation of the bay's ecosystem (Koch et al., 2007; Zieman et al., 1989). Additionally, mangrove forests fringe the bay's edges, serving as vital nursery areas for many marine organisms and provide important coastal protection against erosion and storm surges (Lagomasino et al., 2021). The interplay between seagrass beds, mangroves, and the surrounding waters supports a diverse array of ecological processes, making Florida Bay a crucial and vibrant ecosystem within the greater Everglades region. However, the perennial mortality of seagrass communities in the bay is an ecosystem concern. Since 1987, catastrophic mortality of the *T. testudinum* has been observed in Florida Bay (Carlson et al., 1994; Hall et al., 2016; Zieman et al., 1989), which has been documented as several die-off episodes (Carlson et al., 1994, 2018; Koch et al., 2007, Zieman et al., 1999).

In the summer of 1987, widespread occurrences of dying and deceased *T. testudinum* were documented across most regions of the bay. This decline began near the mudbanks before progressively spreading to affect the entirety of the basin, as detailed by Robble et al. (1991). By late fall of 1990, approximately 94.45 square km of *T. testudinum* were severely affected (Hall et al., 2016; Robble et al., 1991). Yet, as ecological disturbances waned, seagrasses began to slowly

recolonize the bay by the late 1990s (Lapointe et al., 2004). By 2012, the Florida Fish and Wildlife Conservation Commission reported a near-complete recovery of *T. testudinum* in the most heavily impacted basins. However, in 2015, researchers from the National Park Service reported elevated salinities, signs of *T. testudinum* die-off, and the presence of sulfur-rich brine within the affected patches (Hall et al., 2016). Their findings revealed that the 2015 die-off episode spanned approximately 87.77 square km, nearly matching the size and seasonal occurrence of the 1987 event (Hall et al., 2016).

The causal factors of the die-off have been widely debated among scholars. Zieman et al. (1989) put forward protracted drought in southern Florida as the primary contributing factor. However, alternative studies highlighted sulfide toxicity in the sediments (Carlson et al., 1994), hypersalinity of the environment (Fourqurean & Robblee, 1999), chronic hypoxia and action of pathogenic protists (Robblee et al., 1999), anthropogenic nutrient enrichment (Lapointe et al., 2004), extreme disturbance on suspended sediments (Rodemann et al., 2021), and extreme temperature differences (Carlson et al., 2018). These factors occasioned by the complex climate and oceanic actions in the region promote extreme physical conditions that can stress seagrass and ultimately lead to die-off (Nuttall et al., 2000).

SGD significantly influences the physico-chemical condition of estuaries (Black et al., 2009; Kelly et al., 2018), hence it is crucial to assess the dynamics of SGD in Florida Bay and explore its correlation with the seagrass mortality distribution. However, existing studies do not account for the potential relationships between zones of SGD and seagrass mortality. Nonetheless, compelling evidence from various field areas suggests that groundwater influences benthic health (Banda et al., 2023; Robbins, 2023). Hence, there exists a crucial necessity to map the locations of SGD and juxtapose them with the condition of seagrass meadows and the occurrences of seagrass

die-off events within Florida Bay. This drives the focus of our research, aiming to foster a deeper understanding of the coastal ecosystem for both scientific inquiry and management purposes.

1.4.3 Climate Action in Florida Bay

Florida Bay faces complex challenges arising from a combination of natural events and climate change. Its location at the intersection of mainland Florida, the Gulf of Mexico, and the Atlantic Ocean, makes it susceptible to various impacts, ranging from extreme weather events to climate change-driven phenomena. The region's climate is influenced by the El Niño-Southern Oscillation (ENSO) and the Atlantic Multidecadal Oscillation (AMO), which alter sea surface temperatures and precipitation patterns, thereby affecting the bay's environmental dynamics (National Oceanic and Atmospheric Administration, 2023). Warm AMO phases heighten hurricane activity, exemplified by Hurricane Andrew in 1992, which severely impacted the water quality of the Biscayne aquifer, damaging mangrove trees and mudbanks (Blake et al., 2007). The region remains vulnerable to the destructive storm surges and waves that accompany hurricanes (Dessu et al., 2018). The Florida Fish and Wildlife Conservation Commission reported an unprecedented coral bleaching event in the Florida Keys during the summer of 2023, marking the worst recorded instance for the region, which coincided with an El Niño year (Florida Fish and Wildlife Conservation Commission, 2023). The prolonged period of elevated temperatures subjected coral reefs to nearly twice the duration of heat stress compared to previous bleaching events (Florida Fish and Wildlife Conservation Commission, 2023).

Furthermore, drought and sea-level rise stand as prominent climate change-induced threats to Florida Bay. Stabenau et al. (2011) documented a noticeable increase in water levels within the Everglades National Park, mirroring regional sea-level rise trends over recent decades. Carlson et al. (2018) identified climate actions as the primary driver behind elevated temperatures impacting seagrass beds, estuarine circulation, and salinity patterns in the environment. In addition to this,

mud banks are increasing in Florida Bay, which is becoming more saline as Everglades flow and seaward gaps change and the sea level rises (Dessu et al., 2018). The interaction of coastal elevation, sea level rise, and storm-induced surges establishes critical threshold levels that can significantly impact coastal ecosystems and human infrastructure. As sea levels rise due to climate change, these buffer zones are diminished, leading to higher vulnerability. Dessu et al. (2018) opines that breaching these thresholds can lead to significant alterations in coastal topography, hence the urgent need for proactive multidimensional measures to improve the understanding of Florida Bay's ecology and foster resilience against ongoing climate challenges.

1.4.4 Management Efforts in Florida Bay

Due to the complex natural and human-induced impacts on Florida Bay, a multidisciplinary approach was employed to start ecosystem restoration. Over the last Everglades National Park gained international recognition when United Nations Educational, Scientific and Cultural Organization (UNESCO) designated it as a World Heritage Site in 1979 and an International Biosphere Reserve in 1976 (United Nations Educational, Scientific and Cultural Organization, 2018). Following Hurricane Andrew's devastation, UNESCO included the Everglades region, including Florida Bay, on the World Heritage Danger list in 1993 to catalyze global efforts towards ecosystem restoration (United Nations Educational, Scientific and Cultural Organization, 2010). Approximately 1,625 square kilometers within Everglades National Park is managed by the National Park Service, while the remainder falls within the Florida Keys National Marine Sanctuary under the jurisdiction of the National Oceanic and Atmospheric Administration (Stabenau & Kotun, 2012). The U.S. Congress passed the Water Resources Development Act of 2000, providing significant funding through the Comprehensive Everglades Restoration Plan (CERP) to restore, preserve, and protect the South Florida ecosystem (Marshall & Wingard, 2012; Stabenau & Kotun, 2012). This ambitious project, exceeding \$10.5 billion and spanning over 35

years, represents the largest hydrologic restoration effort ever undertaken in the United States (National Park Service, 2016). The CERP identified salinity as “the most important physical parameter in determining species and community composition in south Florida’s coastal water” (Marshall & Wingard, 2012). To safeguard Florida Bay, several management agencies are collaboratively enhancing their understanding of its complex ecosystem dynamics through regular monitoring of hydrological variations and water quality to assess and mitigate environmental threats. This research aims to provide information that would contribute to enhancing management insights.

1.4.5 Survey Site Selection

Three basins within Florida Bay were selected for investigation, viz: Rankin, Whipray and Rabbit Key. Rankin basin, approximately 10.2 square kilometers (Murray et al., 2010), in the central region, is shallowest and nearer to the terrestrial boundary of mainland Florida. Whipray Basin is in the central region, slightly deeper than Rankin and farther away from mainland Florida. Rabbit Key Basin is the deepest, farthest from land and in the western region of Florida Bay (Fig. 1.2). These basins provide ample spatial coverage of the study area, with varying characteristics. The basins faced diverse intensities of *T. testudinum* die-off episodes (Robbins, 2023); however, each responded differently to the prolonged drought that preceded seagrass die-off in 2015 (Hall et al., 2016). Rankin Basin was at the epicenter of the perennial die-off episodes (Robbins, 2023). Whipray Basin and Rabbit Key Basins have a historically moderate die-off intensity (Carlson et al., 2018). These basins were characterized as having areas of patchy to severe seagrass die-off with noted areas of no die-off (Hall et al., 2016) Rankin Basin and Whipray Basin commonly experience hypersalinity, and Rabbit Key Basin has ocean water influence (Lee et al., 2006). The distribution of rainfall across Florida Bay holds significance due to variations in residence time within different basins. For example, in 2009, a two-day, approximately five-inch rainfall event in

May caused the salinity in Whipray Basin to decrease from 44.4 ppt on May 28 to 41.0 ppt on May 31, before rebounding to 44.3 ppt by June 10, thirteen days later (Stabenau and Kotun, 2012). This rapid recovery just two weeks after a rain event suggests that Whipray Basin can have a shorter residence time than the previously estimated 3 - 6-month residence time (Lee et al., 2006).

1.5 Previous SGD Studies in Florida Bay

As Corbett et al. (1999) noted, SGD into Florida Bay is tidally controlled and drives significant nutrients and contaminants into the bay and surrounding keys. Historically, Taylor Slough, situated in the southeastern part of Everglades National Park, supplied most of Florida Bay's freshwater through sheet flow and tidal creeks (Kelble et al., 2007; Orem et al., 1999). This freshwater primarily flows through the mangrove fringes in the northeastern region of Florida Bay (Lee et al., 2006; Nuttle et al., 2000). However, construction and operation of hydrological control structures since the mid-20th century have disrupted freshwater input to the bay (Nuttle et al., 2000; Orem et al., 1999). Due to a significant reduction in freshwater inflows from the Everglades (Corbett et al., 1999; Swarzenski et al., 2009), precipitation has become the primary source of freshwater for Florida Bay. However, on both seasonal and annual timescales, evaporation exceeds precipitation, resulting in a net loss of freshwater from the bay (Carlson et al., 2018; Nuttle et al., 2000; Price et al., 2007). As a result, the bay is seasonally hypersaline (Carlson et al., 2018; Lee et al., 2006). Top et al. (2001) reported that all known wells in the bay produce water with salinity levels comparable to that of the surrounding seawater. In summary, SGD into Florida Bay is influenced by tidal cycles and topographic gradients and contributes significant nutrients and contaminants to the bay. Historically, freshwater inflows have reduced making precipitation the primary source, which, combined with high evaporation rates, leads to seasonal hypersalinity in the bay.

Corbett et al. (2000) estimated the seepage rate of SGD and advective groundwater velocity within Florida Bay. Radon measurements reported between 0.8 to 16 cm/d of SGD (Corbett et al., 2000; Top et al., 2001) while seepage meters produced values ranging from 2 to 40 cm/d (Corbett et al., 1999). These studies suggested that SGD fluxes in the bay originated from the Floridan aquifer. However, Swarzenski et al. (2009) argued that the source of SGD into Florida Bay is likely from shallow sources, with recycled sea waters contributing the main components. The highest fluxes of SGD were observed along the Florida Bay side of the northern Florida Keys (Corbett et al., 1999). Swarzenski et al. (2009) combined geochemical tracers and continuous resistivity surveys to examine the subsurface salinity of the sediments at select SGD outflow locations within the bay. The volume of SGD into Florida Bay remains uncertain, but it is primarily composed of recycled seawater from the adjacent Gulf of Mexico, Florida Strait, and the bay itself (Top et al., 2001).

Surface water salinity in Florida Bay exhibits significant temporal and spatial variability, and is influenced by factors such as precipitation, evaporation, runoff, and exchange with adjacent basins and water bodies (Juster et al., 1997; Kelble et al., 2007). Fourqurean and Robble (1999) linked the hypersalinity of the surface water to cyclic drought conditions in South Florida. Droughts occurring in the 1950s, 1960s, and 1970s resulted in salinity levels of surface waters exceeding 50 ppt in the central regions of Florida Bay by the end of each drought period. The regional drought from 1987 to 1991 led to a gradual increase in surface water salinity throughout Florida Bay, with large areas of central Florida Bay averaging over 50 ppt during the years 1989 to 1990 (Fourqurean et al., 1992).

Enos and Sawastky (1981) hypothesized that the groundwater of Florida Bay is in motion. Juster et al. (1997) tested this hypothesis and discovered that groundwater in the bay is driven by complex processes. The water circulates and sloshes back and forth due to a combination of density

variations, internal instabilities, and the interaction with the underlying rock (Juster et al., 1997). The simultaneous occurrence of seagrass die-offs and hypersalinity drew initial attention to the potential role of hypersalinity, as well as the influence of upstream freshwater diversion, in contributing to seagrass die-off events within Florida Bay.

1.6 Research Questions and Overview of Thesis

I hypothesize that the locations of SGD in the selected study sites will exhibit distinct spatial patterns that vary significantly between wet and dry seasons, with increased SGD activity during the wet season due to enhanced groundwater recharge. Consequently, the overarching goal of this project is to delineate the locations of SGD in Rankin, Whipray, and Rabbit Key Basins, and assess the variations of SGD distribution for both wet and dry seasons within each basin.

The specific questions explored in this research are: 1) what are the locations of SGD in Rankin, Whipray, and Rabbit Key Basins during both wet and dry seasons? 2) how does the distribution of SGD vary between wet and dry seasons within Rankin, Whipray, and Rabbit Key Basins? 3) what are the subsurface characteristics associated with SGD in Rankin, Whipray, and Rabbit Key Basins, as revealed by electrical imaging during wet and dry seasons? 4) how does water quality of SGD differ between the three basins (Rankin, Whipray, and Rabbit Key) across seasonal changes? and 5) what are the key environmental factors influencing the spatial and temporal variations of SGD in Rankin, Whipray, and Rabbit Key Basins throughout the year?

To assess the locations, distribution, and characteristics of SGD within the three basins of interest, I used electrical imaging of subsurface processes during both dry and wet seasons. I employed inversion modeling to generate the resistivity maps of the bulk geologic materials. In-situ measurements of radon and salinity variation were conducted to validate the electrical resistivity datasets. Measured characteristics of the groundwater endmembers helped to explore the research goals. The findings identified and filled significant gaps in the literature and enhanced

the understanding of the utility of electrical imaging in mapping SGD. The variations of SGD will be used to evaluate the distribution of seagrass die-off events and recovery in a future research project.

CHAPTER 2

MATERIALS AND METHODS

2.1 Electrical Resistivity as a Field Data Acquisition Technique in Florida Bay

The distribution of SGD in Florida Bay is underexplored and interaction of SGD with the benthic ecosystem and its contribution to the perennial seagrass die-off in Florida Bay is unknown. Previous studies on SGD in Florida Bay focused on the patterns and quantity of SGD (Corbett et al., 1999). The scarce literature and research of SGD in Florida Bay is partly contributed by the difficulty in detecting SGD. Paepen et al. (2020) argues that the location of SGD in the dynamic environment between land and sea constitutes complexities in detecting and quantifying the flow. The difficulty is also contributed by its spatial and temporal variability (Moore, 1999; Paepen et al., 2020). SGD typically has low specific flux (Burnett et al., 2003; Jou-Claus et al., 2021), as it usually occurs as diffuse seepage rather than focused discharge through identifiable springs (Swarzenski et al., 2004). Thus, mapping SGD demands techniques that minimize uncertainty and produce high resolution data. The use of ER as a proxy to assess hydrological anomalies has been established as a reliable technique for high resolution mapping of SGD (e.g. Fu et al., 2020; Manheim et al., 2004; Swarzenski & Izbicki, 2009). In this study, an ER method that optimizes both lateral and vertical variations of electrical resistivity was used.

2.2 Electrical Resistivity Method Background

The electrical susceptibility of a geologic material is a function of physicochemical properties of the materials. Subsurface electrical properties can be measured by either connecting electrodes directly to the ground (galvanic method) or by inducing an electromagnetic field through the subsurface (inductive method). Electrical resistivity tomography (ERT) is a special kind of galvanic method. Resistivity is a volumetric property that measures how much a material resists the flow of electrical current through it (Rucker et al., 2011). The resistivity of a material

varies indirectly with electrical conductivity; they are reciprocals of each other (Stieglitz et al., 2008). In marine surveys, ERT determines the distribution of physical parameters based on the bulk resistivity characteristics of the subsurface where the subsurface includes the rocks, sediments, porosity, and the porewater or groundwater found within them (Fu et al., 2020). If many measurements of apparent resistivity are taken from the water's surface, ERT can reproduce the scale and resolution required to locate diffuse SGD seepage fields (Cardenas et al., 2010; Fu et al., 2020). One of the drawbacks of ERT is that resistance values generated by modeling electrical resistivity may produce inconsistencies in data sets due to aliasing, suppression, and misidentification of subsurface materials (Johnson et al., 2015). This drawback is amplified in marine systems because SGD interacts with saline water and introduces higher concentrations of conductive particles (Johnson et al., 2015; Manheim et al., 2004). The possibility of using ERT to detect SGD depends on the physicochemical properties of the surface water and groundwater. Conductivity, and therefore salinity is a principal factor that influences the electrical properties of water and is the property that is used to delineate SGD using ERT methods (Manheim et al., 2004). Since resistivity is the inverse of conductivity, higher salinity results in lower resistivity and vice versa. However, if the salinity of surface water and groundwater is almost the same, it would be difficult to identify SGD. Top et al (2001) and Swarzenski et al. (2009) suggested that SGD into Florida Bay mostly comes from shallow sources of recycled seawater, hence it is important to determine if ERT can effectively detect SGD in Florida Bay.

2.3 Electrical Resistivity Profile Collection

Profiles were acquired across Rankin Basin, Whipray Basin, and Rabbit Key Basin in Florida Bay. Each basin was partitioned into gridded lines with a 1000 m by 1000 m spacing (Fig. 2.1) The spacing was selected to maintain good spatial resolution to detect subsurface anomalies using ERT while accomplishing the mapping in a timely manner (approximately two days for the

largest basins). Data were acquired in November 2021 (Rankin and Whipray Basins), June 2022 (Rankin and Whipray Basins) and October 2022 (Rabbit Key Basin). The same 1000 m by 1000 m grid was used to collect wet season and dry season data for Rankin and Whipray Basins making the datasets spatially comparable. Preliminary analysis of the data showed no significant seasonal differences in the Rankin and Whipray Basins. Also, the Rabbit Key Basin did not experience extreme events during the observed periods. Due to these factors and time constraints, I only collected one season's worth of ER profiles for Rabbit Key Basin.

The distribution of marine ER across each basin was mapped using the SuperSting R8 – IP system (Advanced Geosciences, Inc., AGI), equipped with a 66 m long marine resistivity cable that has 22 electrodes spaced 3 m apart (Fig. 2.2). The SuperSting marine system package runs a continuous resistivity profile (CRP) module which measures the ability of current to flow through

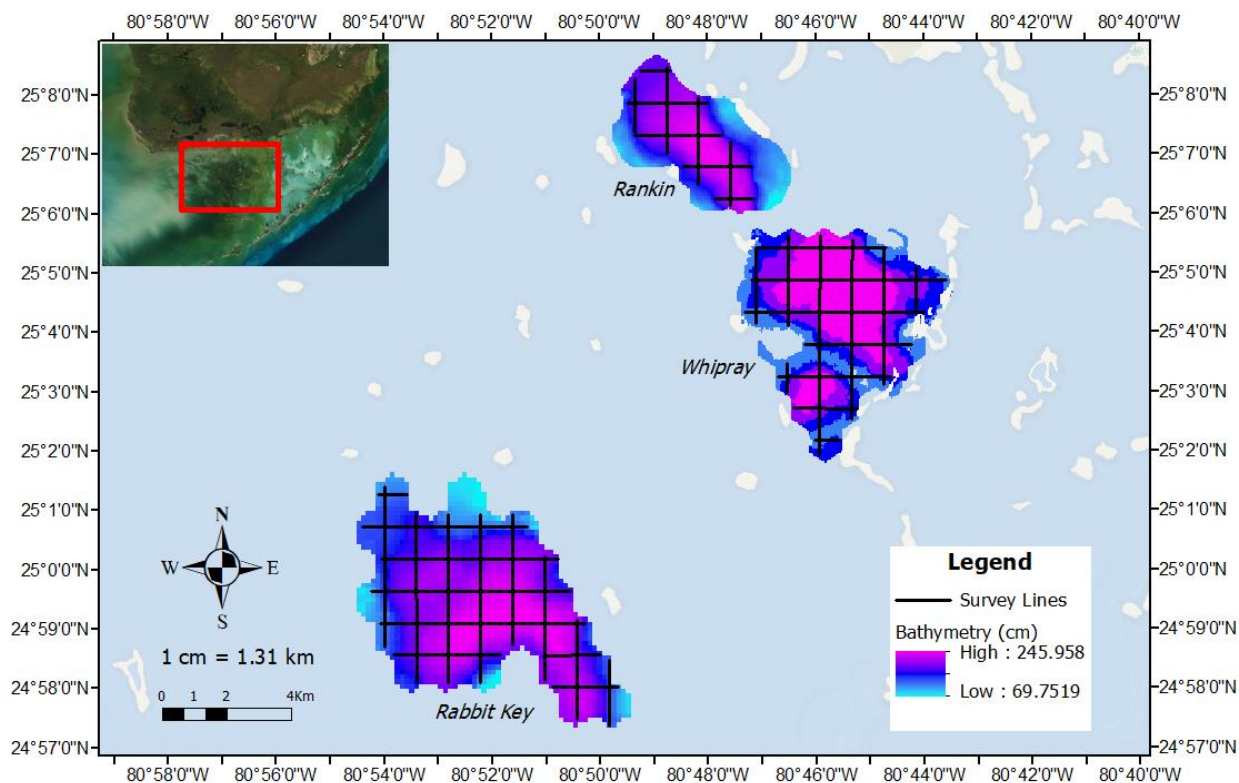


Fig. 2.1: ER data collection survey grids across the three basins (modified from J. Kelly). Bathymetric data courtesy of Dr. Brad Furman.

the surface water into the sub-bottom material (Cross et al., 2011). It uses a heuristic algorithm to minimize the n-factorial route optimization (Advanced Geosciences, 2009). The system employs guided navigation to deal with positioning variables resulting from continuous boat movement (Nyquist et al., 2009). The data are geodetically corrected by the system to check errors inherent in standard conformal projections (Cross et al., 2011). The SuperSting system is designed such that the closest set of electrodes behind the boat are the transmitting dipole and the remaining electrodes are the receiving dipoles (Nyquist et al., 2009). Through the current electrodes (I), electrical current is transmitted into the water column to the sub-bottom materials and the resulting voltage is measured at the remaining potential electrodes (V). I employed a dipole-dipole configuration in the data collection, where two electrodes were designated for fixed current, and voltage potentials were measured across pairs among the remaining 20 electrodes. The dipole-dipole array was used because of its sensitivity to subsurface topography and conductivity variations (Rucker et al., 2011).

During the survey, the marine cable was towed behind a boat ferrying approximately 1.8 m/s. The slow motion of the boat was necessary to acquire high-resolution data (Athanasidou et al., 2009). Foam flotation was attached to the cable



Fig. 2.2: The author in Florida Bay setting up the SuperSting for data acquisition.

between all electrodes to allow the electrodes to only slightly submerge and maintain the electrode depth in the water column during mild sea fluctuations (Cross et al., 2011). The cable was kept taut using a sea anchor. The electric current penetrates to approximately 25% of the length of the towed cable (Cross et al., 2011). Consequently, our system configuration produced ER images that reached a depth of 11.3 meters, covering both the water column and the shallow subsurface. Data was not typically acquired in areas where the water depth was less than 0.6 m, to minimize noise and scattered data. The SuperSting recording system stores the apparent resistivity values, representing volume-averaged values that consider all geologic layers through which the induced current flows. Several files are recorded at each line of data acquisition including STG (.stg), GPS (.gps), and DEPTH (.dep) files. The STG file contains the resistivity measured for each electrode across the survey field. It also incorporates the date, navigation speed, coordinates of the electrodes, output currents, and percentage errors. The GPS file contains the geodetic reference of the navigation, water depths, and water temperature that were collected using a HDS5 Lowrance GPS device, which was connected to the SuperSting. During surveys, the Lowrance GPS device also captured depth data via transducer mounted on the boat's transom just below the water's surface.

Before starting the ERT survey, thorough equipment calibration was carried out. The calibration was performed to ensure the measurements align with established standards, reducing bias and inaccuracies. All cable connections were fastened appropriately to avoid energy dissipation and errors in readings. The voltage levels, current reading and settings were checked to match values recommended by the equipment manufacturer. Quality control checks on the relay, receiver, and cable were also conducted before data collection. The cable was kept straight throughout the survey using a sea anchor to ensure accurate measurements of the subsurface resistivity. Errors in data collection can stem from various sources, including misalignments of the

electrode streamer caused by water currents, which can lead to inaccuracies in electrode positioning relative to the desired survey layout (Arboleda-Zapata et al., 2022). In wavy conditions, vertical oscillation of electrodes can disrupt complete contact with the water surface, affecting measurement accuracy (Arboleda-Zapata et al., 2022). Average wind speed during the surveys, both wet and dry seasons, varied from 2.7 to 5.9 m/s, equating to sea state 2 to 4 “light breeze to moderate breeze” (National Weather Service, n.d.). Bay water was noticeably choppy at some intervals.

2.4 Ground Truth Data Collection

Electrical conductivity of groundwater is facilitated by ions, therefore, the values of ERT data depend on the chemical and physical properties of the material through which groundwater flows (Manheim et al., 2004). The SuperSting system records apparent resistivity values, which represent bulk resistivity — a composite of water content, physical processes, and geological materials within the measurement area. Hence, conductivity measurements of groundwater endmembers are necessary to ground truth the ERT data.

Following the preliminary processing and interpretation of ERT data (to be discussed in chapter 3), areas exhibiting spikes in resistivity readings higher than the background readings were identified as potential SGD zones. These anomalous zones were documented for closer analysis. The delineation of “anomalous” (referred to as “A”) and “normal” (referred to as “N”) zones ensued through a visual analysis of ERT signatures within each basin. An “A” zone was characterized by elevated resistivity exhibiting spikes extending from the limestone layer to the water surface, surrounded by a comparatively uniform resistivity backdrop. The width of these anomalies typically ranges from 0.3 m to 2.5 m, with varying depths within the carbonate mud and some extending to the limestone units. The “N” zones were chosen from the background readings within a 20-meter radius of the anomalous area and served as a control group for the ground truth.

Subsequently, five representative "A" and "N" locations were selected from each basin for ground truthing (n =15 A and 15 N total).

During the ground truth data collection, I ensured that the sampling was as close to the observed coordinate as possible. However, owing to slight oscillation of the boat, it was difficult to pinpoint the exact coordinates, hence I ensured the collection was within 5 m of the coordinates of interest. From the "A" and "N" locations. Since visual inspection showed resistivity differences between the "A" and "N" areas, salinity was the targeted proxy for ground truth because salinity influences the electrical resistivity of the material. I collected water quality data instead of geological samples because water quality directly provides information on salinity and radon content of the groundwater. This method is faster, more efficient, and less invasive than geological material sampling, allowing for immediate assessments and quicker laboratory analysis. Moreso, extracting sediments from the bay requires extra permits and regulations.

Water quality data, including temperature, salinity, conductivity, pH, and dissolved oxygen, are essential for accurate SGD characterization (Kelly et al., 2018). Ten groundwater samples were collected from each of the basins (n=30 total) in the wet season. All groundwater samples were collected using a 2 m push-point piezometer (M.H.E. products) connected to a peristaltic pump (Geotech) by masterflex tubing. The piezometer was pushed through the carbonate muds down to the limestone, typically 25 to 145 cm deep. I measured temperature, pH, salinity, and conductivity of each groundwater sample using YSI Model 63 (YSI Inc., Yellow Springs, OH) connected to a flow through cell. Prior to sample collection, the water quality meter was calibrated with factory-supplied solutions. The sediment thickness and water column depth at each groundwater sampling site were also recorded. As described in Chapter 1, radon-222, which has a half-life of 3.8 d is a reliable tracer of SGD (e.g. Burnett & Dulaiova, 2003). Groundwater

samples for radon-222 analysis were collected from all 30 ground truth sites in 250 mL screw-top glass bottles with no head space using the piezometer and pump set-up described above.

CHAPTER 3

DATA PROCESSING, ANALYSIS, AND RESULTS

3.1 Electrical Resistivity Profile Processing

All ERT datasets were downloaded from the SuperSting system to a hard drive. The data were imported into the SuperSting Marine Log Manager (Advanced Geosciences, Inc.) for processing. Quality control was implemented to ensure accuracy and reliability of the data. In resistivity surveys, it is standard practice to remove negative apparent resistivity values (Advanced Geosciences, 2009). A threshold of 0.1 to 1.0 Ωm was therefore applied to filter out negative values (Advanced Geosciences, 2009). GPS files were visualized using a GPS visualizer in Marine Log Manager to keep track of the navigation, which aided in edge cutting and termination zones so that only straight segments were processed, thereby minimizing errors that occurred from deviations in a survey route (Manheim et al., 2004). The Marine Log Manager software allowed for the editing and merging of the STG and GPS files. By merging the navigation file with the resistivity data, a linearized STG file was generated. Linearization addresses the irregular variations in subsurface resistivity and the non-linear relationship between electrode potential and the subsurface (Cross et al., 2011). Subsequently, these linearized data were exported in a format compatible with EarthImager 2D inversion software (Advanced Geosciences, Inc.), yielding a linearized STG containing the resistivity information and a DEPTH file containing the bathymetric data.

EarthImager 2D software runs a Gauss-Newton algorithm for non-linear least square optimization (Advanced Geosciences, 2009). In the software, the subsurface was discretized into a series of rectangular blocks, and the resistivity of each of these blocks was estimated (Cross et al., 2011), yielding an apparent resistivity pseudosection that aligns with the measured apparent resistivity values obtained from the survey. By integrating data on water depth into the modeling

process, the software refines the resistivity estimates and produces a more precise resistivity profile of the subsurface. Before inversion, the software environment was set to salt-water to ensure the algorithm recognized the physical environment where the data was obtained from. The minimum resistivity value was set to $0.1 \Omega\text{m}$ because seawater resistivity can be as low as $0.1 \Omega\text{m}$. By imposing a minimum resistivity threshold, the inversion process maintains stability and convergence towards a physically plausible solution (Nyquist et al., 2009). This approach helps prevent artifacts or anomalies in the resistivity model that could arise from overly low resistivity values in the inversion process (Advanced Geosciences, 2009). The maximum number of iterations was set at seven to obtain optimal inversion, in line with the specifications of Fu et al. (2020).

To start inversion, the linearized STG file was imported into the EarthImager 2D. The DEPTH file was loaded to provide the depth and temperature readings of the water column. The EarthImager 2D CRP module handles extensive volumes of continuous resistivity data, mimicking a "divide-and-conquer" strategy, where the lengthy section of a single collection file was segmented into numerous subsections (Cross et al., 2011). The inversion took from five minutes to one hour to process each line, depending on the line length and data quality. Each subsection undergoes individual inversion, and the process concludes by consolidating the subsections into a unified profile (Advanced Geosciences, 2009). The STG file undergoes iterative linearization, through which the algorithm calculates the resistivity of the subsurface at each electrode iteratively, considering the resistivity of the surrounding electrodes (Advanced Geosciences, 2009). This process delinearizes the data, which produces a two-dimensional resistivity model of the subsurface. The models are generated individually for each electrode, as well as a segment that considers the entire line as a unified section. The outputs are sections for the measured apparent resistivity pseudosection, calculated apparent resistivity pseudosection, and inverted resistivity

section. Three types of files are generated during the processing: JPEG images of the complete resistivity profile, including long (uncompressed) and short (compressed) versions for each line, providing both detailed and overview visual representations; text files of processed resistivity data, comprising XYZ files with distance along the line (x), depth (y), and resistivity values (z), LLT files containing longitude, latitude, depth, and resistivity values for georeferenced analysis; and an INI file that stores processing parameters used, facilitating consistency in parameter settings for subsequent processing. The JPEG images generated through the EarthImager 2D processing were stored using the default color scale. This scale spans a gradient from blue tones to red tones, where the red hues correspond to higher resistivity values and blue hues have lower resistivity values (Fig. 3.1). Every step of this process was saved into an individual folder corresponding to each

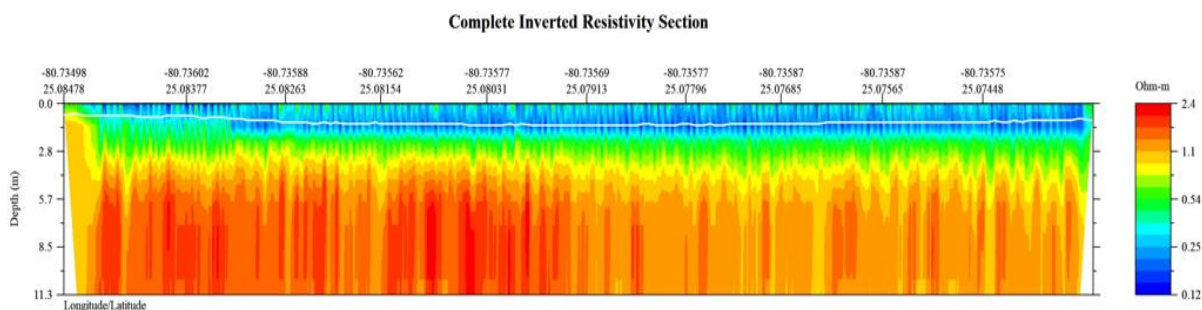


Fig. 3.1: Typical inverted section of a single ER line. The white line shows the sediment-water interface.

line

of collected data.

The EarthImager 2D software displays predictive statistics of the inversion in the inverted resistivity section (Fig. 3.2). The root mean square (RMS) and L2-norm values, which show how the model performed, were recorded for each iteration. RMS is a statistical measure on the goodness of fit between the measured resistivity and the inverted resistivity model (Advanced Geosciences, Inc., 2009). Lower RMS values show better fit. The L2-norm also quantifies data misfit, calculated as the sum of the squared weighted data errors. Lower values of L2-norm indicate better models. Noise and data misfits result in large values of RMS and L2-norm. To correct poor

models, a data histogram was generated to visualize the misfit. Outliers were visually identified and removed. The data were saved and reinverted until the RMS and L2-norm reached acceptable values. In marine surveys, a satisfactory fit is typically achieved when the RMS error is below 10% and the L2-norm value is less than 5% (Dimova et al., 2012). All the acquired ERT datasets

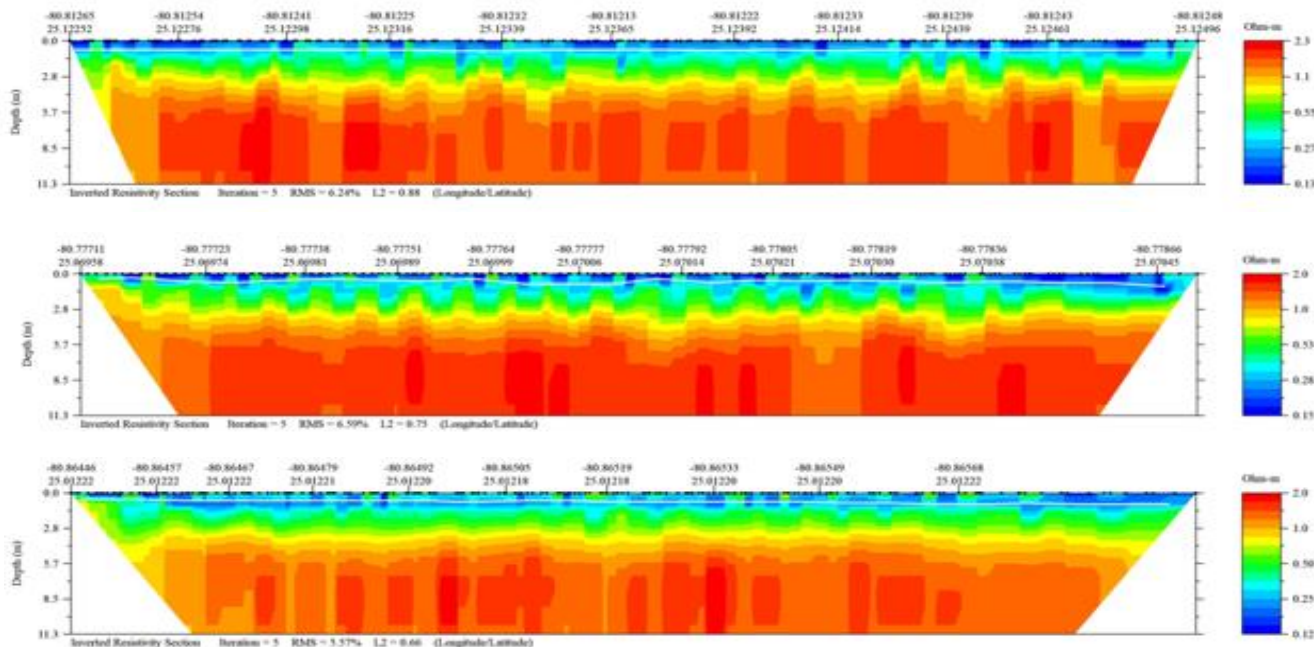


Fig. 3.2: Inverted resistivity sections for the basins with modeling statistics. The “white line” marks the bathymetry. Top: Rankin Basin, Middle: Whipray Basin, Bottom: Rabbit Key Basin

were inverted, and the models were validated appropriately. However, some data sections with significant noise were unable to be inverted. Models showing deficiencies, such as high RMS (greater than 10%), along with sections containing more than 5% missing data, were excluded to maintain the reliability and validity of the analysis.

3.2 Results of Electrical Resistivity Profiles

The bulk resistivity of the ER profile typically spans from 0.1 to 2.2 Ωm (Figures 3.2 and 3.3). The highest resistivity value recorded, while maintaining acceptable RMS and L2-norm, was 4.5 Ωm. Three distinct layers were identified in the ER profiles. Integration of the water depth data

into the inversion process allowed for the delineation of areas above the baseline as water column, which are characterized by the lowest resistivity readings, typically ranging from 0.1 to 0.35 Ωm . Most of the inverted ER profiles yield a resistivity close to 0.2 Ωm for the water column (blue hues), which aligns closely with the resistivity expected for seawater (Cardenas et al., 2010). The layer of carbonate mud, with resistivity values approximately between 0.35 to 1.2 Ωm , is visually represented by green and yellow color gradients. The carbonate mud layer hosts the root systems of the seagrass meadows. The Miami Limestone formation, below the mud, exhibits the highest resistivity, typically exceeding 1.2 Ωm . There was no observable difference in ER datasets

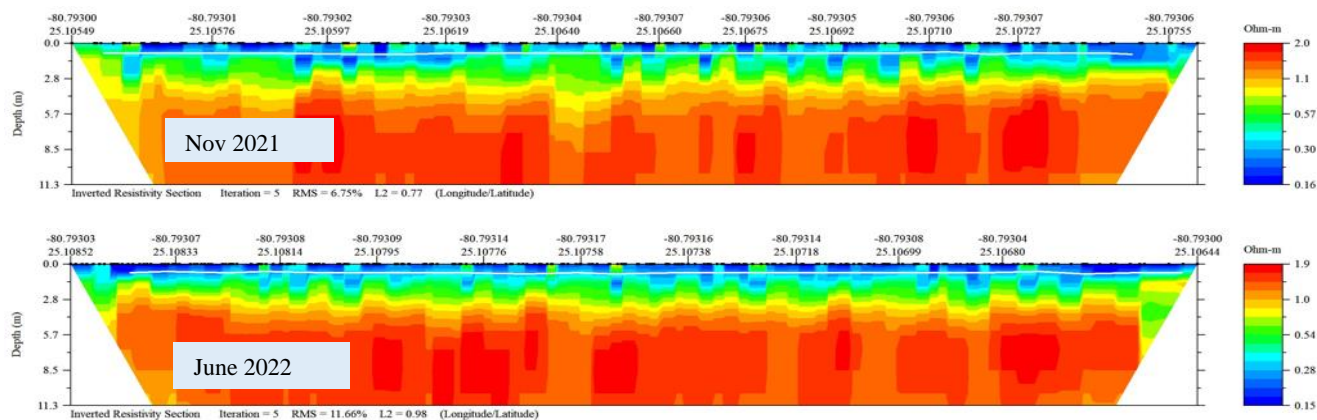


Fig. 3.3: Inverted section of Rankin taken in November 2021 (dry season) and June 2022 (wet season). There was no significant difference between the two season and years. Note: The resistivity scale varies slightly between profiles. The white line delineates the sediment-water interface.

obtained from each basin.

Datasets from the wet and dry seasons of 2021 and 2022 were selected for a time series analysis. To maintain consistency, I ensured that the datasets were from the same locations and possessed closely matching descriptive statistics. Nevertheless, the analysis of inverted resistivity sections from each season revealed minimal variations in resistivity across the years. Both the resistivity and depth of penetration remained consistently uniform between the two years, with areas displaying similar readings showing little change between seasons (Fig 3.3). Consequently,

there was no need for conducting a second ERT survey of Rabbit Key Basin in 2023. Thus, the interpretation of datasets is based on the 2021 and 2022 datasets acquired across the basins.

3.3 Geospatial Analysis of Groundwater Sample Locations

As specified in section 2.4, salinity and radon groundwater samples were collected from "A" (anomalous) and "N" (normal) sites within each basin. The actual field sampling locations of all "A" and "N" sites were compared with their intended sampling locations. Positional discrepancies were then calculated between the intended and actual sampling locations (Table 3.0). I then established a quality control protocol to verify that the ground truth records for both "A" and "N" were accurately captured within their respective designated areas. This involved visually assessing each "A" site relative to the ER data to ensure the actual sampling location was within an anomaly area on the ER data. Furthermore, we cross-checked that the "N" sites were not in anomaly zones on the ER data. During this process, the location for "A" at site W8 in Whipray Basin deviated by 18 m from its expected position. Consequently, W8A was excluded from further analysis. All other sampling points were collected from within their respective "A" and "N" zones.

Table 3.0: Record of the salinity and radon-222 activity measured for "A" and "N" locations. The "B", "R" and "W" in the name field represent Rabbit Key, Rankin and Whipray basins respectively. The 'Target' column lists the expected coordinates, while the "Actual" column reports the actual coordinates obtained during ground truth survey. The "difference" column reflects the discrepancies between observed and field coordinates.

Name	Salinity (ppt)	Radon (Bq/m³)	Target (Latitude and Longitude)	Actual (Latitude and Longitude)	Difference (m)
B2A	37.3	326	25.003045, -80.897101	25.003033, -80.897117	2
B2N	38.0	99	25.002996, -80.896482	25.003017, -80.896467	3
B4A	39.9	263	24.986080, -80.900312	24.98605, -80.900333	5
B4N	39.5	100	24.979091, -80.900183	24.979167, -80.900133	9
B5A	40.3	51	24.975602, -80.870041	24.975617, -80.870033	2
B5N	38.8	351	24.976130, -80.866879	24.976180, -80.86695	8
B8A	39.7	207	24.954211, -80.836039	24.954167, -80.836117	9
B8N	41.5	109	24.954170, -80.835818	24.954217, -80.835800	6
B11A	39.0	220	25.016980, -80.900006	25.017033, -80.900051	6
B11N	39.8	100	25.011981, -80.90008	25.012050, -80.900033	9
R4A	40.7	222	25.117149, -80.792818	25.117133, -80.792833	2
R4N	44.9	60	25.116490, -80.792911	25.116533, -80.793001	12

R5A	38.0	37	25.104301, -80.793020	25.104217, -80.79312	2
R5N	42.7	168	25.104252, -80.793269	25.104251, -80.793167	1
R8A	44.3	138	25.134112, -80.822618	25.134049, -80.822583	4
R8N	44.1	215	25.134591, -80.822640	25.134583, -80.822633	0
R9A	43.8	93	25.112962, -80.803040	25.113011, -80.803083	7
R9N	44.6	77	25.113293, -80.803079	25.113283, -80.803133	5
R10A	44.0	201	25.131481, -80.802670	25.131467, -80.802717	5
R10N	42.7	200	25.131212, -80.803840	25.131317, -80.803805	13
W1A	34.1	63	25.079120, -80.775320	25.079117, -80.775317	0
W1N	30.0	421	25.079494, -80.775331	25.079517, -80.775333	3
W3A	33.3	159	25.076924, -80.785291	25.076921, -80.785272	4
W3N	34.1	54	25.077741, -80.785352	25.077751, -80.785317	3
W6A	39.9	121	25.081323, -80.742211	25.081133, -80.741901	3
W6N	26.9	299	25.081334, -80.742012	25.081317, -80.742016	3
W8A	32.7	291	25.075360, -80.7358197	25.075214, -80.735817	18
W8N	29.2	389	25.075632, -80.735871	25.075667, -80.735883	4
W10A	27.6	157	25.081531, -80.755774	25.081517, -80.755833	7
W10N	27.8	102	25.081570, -80.755522	25.081600, -80.755567	6

3.4 Radon Data Processing

Radon samples were analyzed within three days of collection using a RAD-H2O system (Durrige Company Inc.), given radon-222 has a short half-life of 3.8 days. Following analysis, a decay correction was applied to adjust the counts to account for the time elapsed between sample collection and analysis. This ensures that the reported radon-222 activity accurately reflects the radon present in the groundwater at the time of sampling. The storage of samples in screw-top glass bottles and silica septa to avoid outgassing and their analysis within three days to minimize decay are both crucial for maintaining the integrity and accuracy of the measurements (Jobbágy et al., 2019). Humidity during the analysis can affect radon-222 measurements. Samples were analyzed once relative humidity in the RAD7 was low. Capture software (Durrige Inc.) was used to humidity correct all analyses of radon-222 in groundwater. The decay-corrected radon-222 values were calculated using the formula:

$$C_{corr} = C_{meas} \times e^{(-\lambda t)}$$

C_{corr} = Decay-corrected radon-222 concentration

C_{meas} = Measured radon-222 count rate

λ = Decay constant for radon-222 ($\lambda \approx 0.693 \text{ day}^{-1}$)

t = Time elapsed between sample collection and analysis (in days)

3.5 Results of Groundwater Data

The analysis of groundwater endmembers across various basins revealed salinity levels surpassing those of surface seawater. The average groundwater salinity measured was 39.9 ppt ($n = 30$), nearing the threshold for hypersalinity defined as 40 ppt by Stabenau and Kotun (2012), indicating widespread near-hypersaline conditions within the bay's groundwater. In Rankin Basin, the groundwater was hypersaline, with average salinities of 42.2 ppt ($n = 5$) in zone "A" and 43.6 ppt ($n = 5$) in zone "N". The standard deviations were 2.5 and 0.9, respectively. Groundwater salinity in this basin peaked at 44.9 ppt. Whipray Basin exhibited lower mean salinities of 33.5 ppt ($n = 5$) in zone "A" and 29.6 ppt ($n = 5$) in zone "N", with standard deviations of 4.2 and 2.5, respectively. In Rabbit Key Basin, zone "A" recorded an average salinity of 39.2 ppt ($n = 5$), while zone "N" averaged 39.5 ppt ($n = 5$). The standard deviations were 1.1 and 1.2 for zones "A" and "N", respectively.

Furthermore, the analysis of radon activity indicated variations between zones "A" and "N" within each basin, suggesting potential differences in groundwater presence or groundwater residence time. In Rankin Basin, mean radon activity was 138 Bq/m³ ($n = 5$) in zone "A" with a standard deviation of 68, and slightly higher at 144 Bq/m³ ($n = 5$) in zone "N" with a standard deviation of 64. Conversely, both zones in Whipray Basin displayed elevated radon activity, with zone "A" averaging 158 Bq/m³ ($n = 5$) and zone "N" averaging 253 Bq/m³ ($n = 5$). The respective standard deviations were 75 and 150. Interestingly, the "A" zones in Rabbit Key Basin showed higher radon activity levels compared to "N" zones, with average readings of 213 Bq/m³ ($n = 5$) and 152 Bq/m³ ($n = 5$), respectively. The standard deviations for zones "A" and "N" were 91 and 105, respectively.

3.6 Statistical Analysis of Groundwater Samples

I conducted parametric and non-parametric statistical analyses to evaluate potential differences between “A” and “N” measurements for both salinity and in-situ radon datasets. The tests were conducted to identify significant shifts in salinity and radon activity that could be attributed to factors influencing the anomalies observed in the "A" sites relative to “N” sites. First, I performed a parametric test with the assumption of normality to understand the distribution of the “A” and “N” datasets. I tested for normality using the Shapiro-Wilk test. If the datasets were normally distributed, I conducted a t-test to compare the means of the anomalous and normal measurements. When the datasets were not normally distributed, I used the Wilcoxon signed-rank test. These tests were initially conducted for “A” and “N” measurements in each basin to investigate local patterns and then pooled analysis across all basins to gain a broader understanding of the regional variations. The Wilcoxon signed-rank test was not conducted for the radon datasets because the Shapiro-Wilk test indicated that all the datasets from each basin followed a normal distribution. A p-value threshold of 0.05 was used to determine statistical significance (Hagedorn & Tsuda, 2022), meaning that results with p-values less than or equal to 0.05 were considered statistically significant. This indicates a less than 5% probability that the observed differences were due to random chance.

All statistical analyses were conducted using Python programming on Google Colab. I employed a combination of Python libraries to process data, conduct statistical tests, and visualize results. The framework and applicability of these Python tools in geoscience studies are comprehensively discussed by Morra (2018). NumPy facilitated efficient manipulation of data arrays and provided essential mathematical functions for statistical calculations. SciPy was instrumental in performing advanced statistical tests. Matplotlib and Seaborn were utilized for data visualization, allowing generation of informative plots such as scatter plots to explore the

distribution of salinity and radon data, identify patterns, and visually assess the significance of differences between salinity in anomalous and normal areas across basins.

Table 3.1: P-values for the test statistics for salinity (significance at $\alpha = 0.05$ denoted by *). Tests were not run for data marked as X.

Basins	Shapiro-Wilk	T-test	Wilcoxon-Signed
Rankin	0.0176*	X	0.4375
Whipray	0.3044	0.2260	X
Rabbit Key	0.9372	0.7315	X
Pooled	0.0056*	X	0.9775

Table 3.2: Statistics for radon activity in the basin. The values recorded are p-values with significance at $\alpha = 0.05$ denoted by *). Tests were not run for data marked as X.

Basins	Shapiro-Wilk	T-test	Wilcoxon-Signed
Rankin	0.2133	0.9041	X
Whipray	0.2036	0.2889	X
Rabbit Key	0.2352	0.4010	X
Pooled	0.0473*	X	1.0000

The p-values obtained from salinity and radon comparisons between the “A” and “N” sites provide insights into the variability of salinity and radon patterns. Significantly low p-values, denoted by asterisks, indicate substantial differences in salinity (Table 3.1) and radon-222 activity (Table 3.2). Conversely, non-significant p-values suggest relative homogeneity in salinity or radon activity, although subtle variations may still exist but are negligible. The Shapiro-Wilk test revealed a significant p-value (less than 0.05) for Rankin Basin salinity and the pooled datasets, indicating deviations from a normal distribution (Table 3.1). To further investigate, a Wilcoxon-signed test, a non-parametric analysis, was employed to determine if the population mean of the “A” zones differed from the “N” zones. The results showed no significant difference in salinity between the “A” and “N” zones in both Rankin Basin and the pooled data for the three basins (Table 3.1). This suggests non-unique salinity patterns within the “A” and “N” zones in Rankin Basin, indicating similar water chemistry across the basin. Also, the pooled salinity data show no significant difference between the “A” and “N” zones across all basins, suggesting a homogeneous

salinity regime in Florida Bay. Moreover, there was no significant difference in the salinity data between the “A” and “N” zones in Whipray and Rabbit Key Basins (Fig. 3.1), indicating non-unique salinity patterns in both the anomaly and background zones (see Fig A.1 in appendices). These findings suggest that these basins might be experiencing consistent hydrological conditions or less complex interactions between freshwater and saltwater inputs.

The Shapiro-Wilk test was conducted to assess the normality of radon activity distributions within each basin individually, as well as for the pooled dataset. The results indicated that radon activity was normally distributed across all basins, but not with the pooled data (Table 3.2). Consequently, a t-test was employed to compare the mean radon activity between the "A" and "N" zones within each basin, aiming to determine if there were significant differences between these zones. The t-test results revealed no significant difference in radon activity between the "A" and "N" zones, suggesting that radon activity in the anomalous zones does not deviate substantially from the background levels in any of the basins. Also, the Shapiro-Wilk test for the pooled mean radon activity across all basins indicated that the data were not normally distributed at $\alpha = 0.05$ (Table 3.2). Therefore, a Wilcoxon-signed test was conducted on the pooled data to determine if the population mean of the “A” zones differed from that of the “N” zones. The Wilcoxon-signed test results showed no significant difference in radon activity between the “A” and “N” zones for the aggregated data. This suggests a homogeneous distribution of radon activity in both the “A” and “N” zones across the basins.

CHAPTER 4

INTERPRETATION OF RESULTS AND DISCUSSION

4.1 Electrical Resistivity Profiles

Preliminary findings from the time series analysis of the datasets collected during the wet and dry seasons of 2021 and 2022 provided insights into the temporal stability of the geophysical properties of the surveyed area. First, the data consistency across the three basins suggests that despite seasonal variations in tides, temperature, and rainfall, the inverted resistivity sections remained consistently similar over two consecutive years, indicating that surficial processes did not significantly impact subsurface resistivity properties. Second, this stability is further supported by the consistent measurements of resistivity which did not vary significantly between the wet and dry seasons or from one year to the next. There was no record of drastic land use modification or extreme events, such as hurricanes, impacting the bay during the two years of observation. These disturbances might introduce variability not captured in this bi-annual snapshot. The observed consistency in resistivity across different seasons and successive years can likely be attributed to the low precipitation and prolonged water residence time in the bay (Fredley et al., 2019; Shank et al., 2011). The negligible variance observed might also be attributed to the lack of freshwater input from the mainland Everglades into the bay, as runoff from Florida mainland into the bay is minimal due to historical water management practices (Fredley et al., 2019; Nuttle et al., 2000; Top et al., 2001).

In the ER profile as described in section 3.2, the variations in resistivity between the layers are influenced by several factors, including organic content variability, compaction, the porosity network, and the composition of water filling pore space (e.g. Fig. 4.1; Tassy et al. 2014). The topmost layer, characterized by the lowest resistivity, represents the water column. The high seawater content in this layer made it a good conductor of electricity, hence it maintained the

lowest resistivity in the profile. Seawater itself typically exhibits resistivity ranging from 0.1 to 0.2 Ωm , with occasional fluctuations due to variations in salinity and temperature (Cardenas et al., 2010). The carbonate mud layer consists of a mixture of water and sediment particles, with the water content playing a significant role in determining its resistivity (Sun et al., 2023). During groundwater sample collection, the average depths of carbonate muds were 0.9 m in Rankin, 0.5 m in Whipray, and 1.1 m in Rabbit Key Basins. These measurements, ranging from 0.5 to 1.1 m, align with the typical depths observed in the ER profiles below the delineating white line of the water column (Fig. 4.1).

The presence of submerged aquatic vegetation (SAV) and clay minerals within the mud could contribute to its electrical conductivity compared to seawater. Variations in resistivity values at the sediment-water interface are likely influenced by SAV. While our study area's relationship between electrical resistivity and SAV remains unclear, research by Amato et al. (2010) indicates

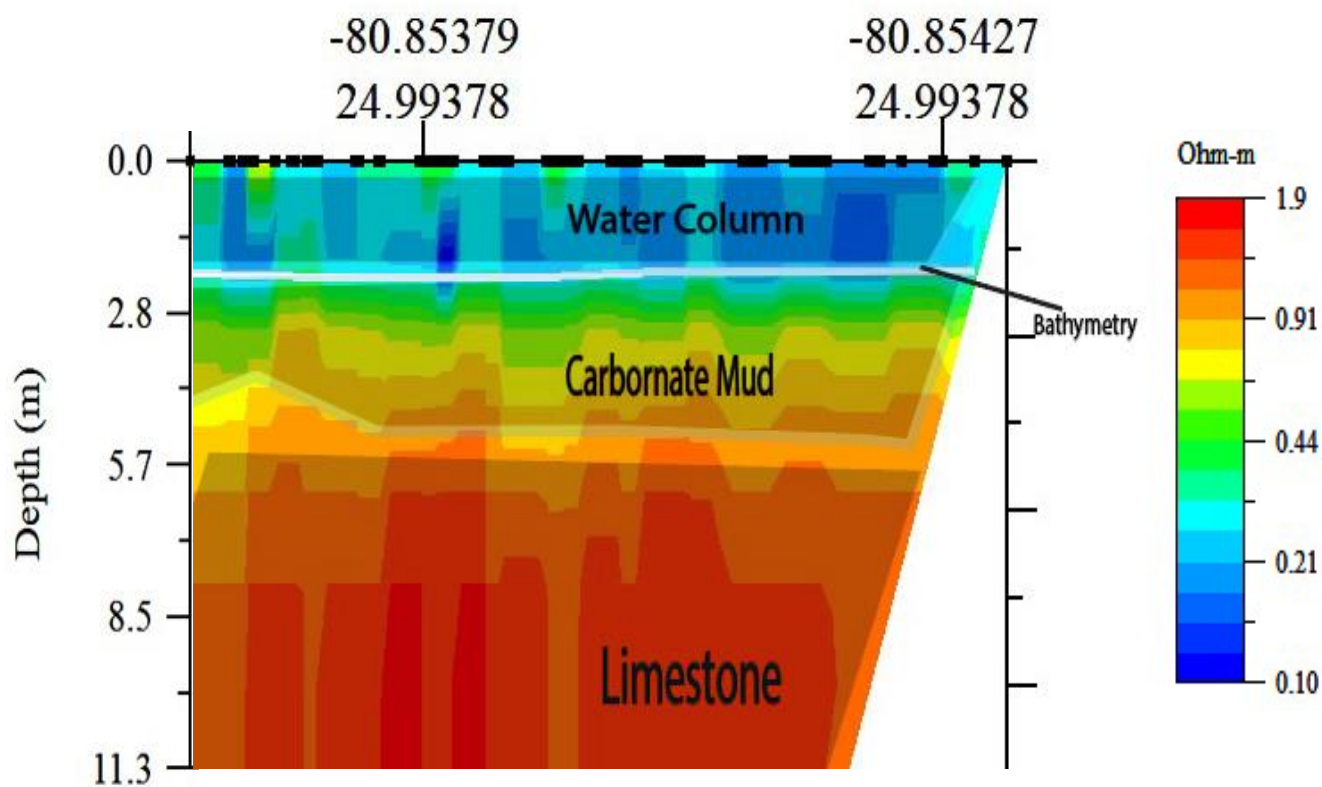


Fig 4.1: Layers identified from the ER profile, showing water column, carbonate mud and limestone members.

that root biomass affects resistivity. Amato et al. (2008) observed that increased herbaceous plant root density generally raises soil resistivity, yet they emphasized the necessity for site-specific calibrations due to ambiguity inherent in 2D geoelectrical surveys. I propose that the root structure of SAV forms water-filled channels with varying salinity, resulting in a wider range of resistivity (0.35 to 1.2 Ωm) depicted by tones ranging from green to yellow (Fig. 4.1).

While typical resistivity values for wet limestone can range widely from 50 to 1,000 Ωm (Griffiths & Barker, 1993), the presence of saline to hypersaline groundwater (Table 3.0) significantly lowers this reading in our field area. As observed by Griffiths and Barker (1993) in Staffordshire, England, saline groundwater zones exhibited resistivity as low as 5 Ωm , while background rock formations showed values around 100 Ωm , highlighting the strong influence of salinity on resistivity readings. The salinity of the Miami Limestone in Florida Bay exhibits historical and spatial variations, largely due to the dynamic interactions within the aquifer system (Marshall & Wingard, 2012). The high salt content of the groundwater indicates that the Miami Limestone formation is saliferous, contributing to the low resistivity observed. Marshall & Wingard (2012) discovered a predominance of euryhaline species in the benthic zone of Florida Bay, aligning with the region's salinity characteristics. Compared with the other layers in the ER profile, the elevated resistivity readings in limestone layers stem from their low porosity, restricting the presence of conductive fluids due to limited water storage space (Robert et al., 2011). Moreso, the mineral composition of limestone contributes to its resistivity, compared to water or clay-rich sediments (Schulmeister et al., 2003).

The bulk resistivity values observed fall within the anticipated range for surveys conducted in carbonate marine environments, echoing findings from research conducted in northeast Florida Bay by Swarzenski et al. (2009), situated close to the mainland Everglades. This consistency suggests a relatively homogeneous geological composition and consistent electrical properties

throughout Florida Bay. Drawing from established resistivity-porosity relationships, such as Archie's Law for carbonates (Archie, 1942), I can expect the bulk resistivity of seawater-saturated unconsolidated carbonates in Florida Bay to range between 0.4 and 0.5 Ωm (Jackson et al., 2002), with potential peaks reaching 1 Ωm .

As discussed in Section 2.4, I identified pockets of hypersaline groundwater exhibiting low resistivity (Fig. 4.2; left panel). I also observed resistivity spikes or upwells emanating from the seafloor and extending into the water column (Fig. 4.2, right panel). Given the prevalence of unconsolidated sediments in the seafloor, I characterized the zones with spikes in resistivity as potential zones where fresher waters could ingress into the seawater, thus creating the sharp differences in resistivity. As noted earlier, the ERT relies on salt solutions as electrolytes to image the subsurface, hence the observed spikes might indicate areas where fresher water is mixing with seawater, resulting in distinct resistivity contrasts. I make this deduction as freshwater typically

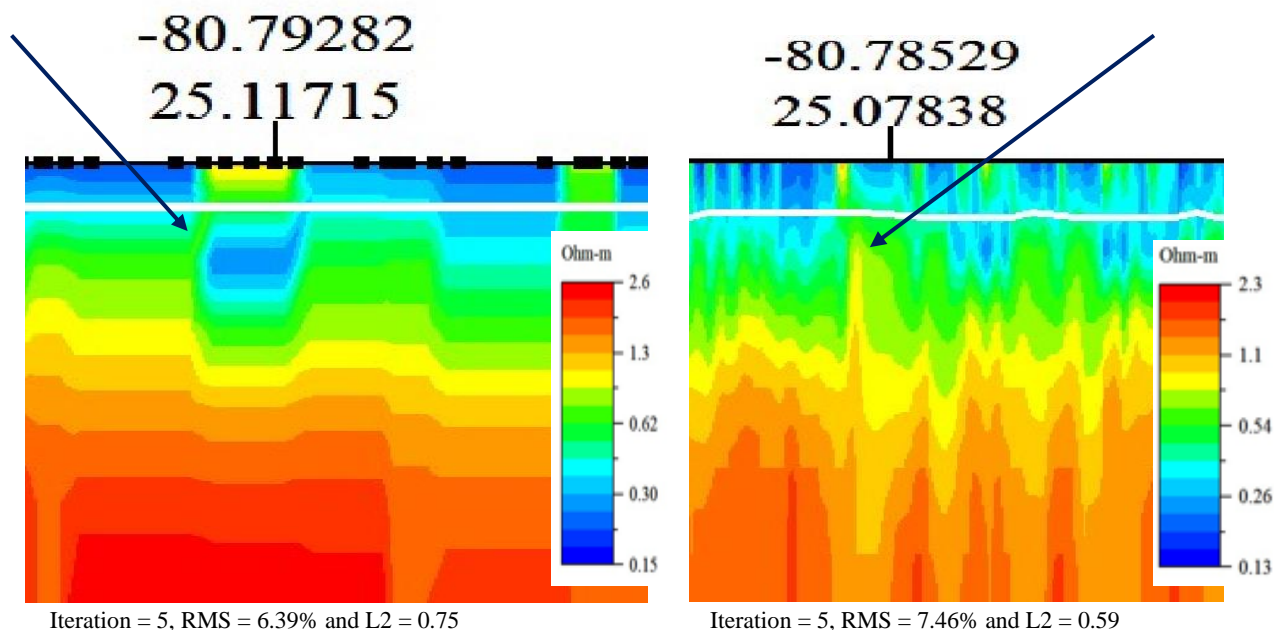


Fig. 4.2: Detected anomalies in different portions of the basins marked by elevated resistivity upwelling from the limestone to the water column. Left panel: Pocket of saline SGD characterized by blue anomaly surrounded by greenish yellow. Right panel: Karstic structures upwelling from the limestone unit to the water column.

exhibits higher resistivity than seawater due to its lower salt content. For example, Paepen et al. (2020) found freshwater in areas along the Belgian coast with resistivity values exceeding $20 \Omega\text{m}$, while saltwater areas showed resistivity below approximately $2.5 \Omega\text{m}$. Similarly, Attias et al. (2020) identified pools of freshened water within a conductive saline background in the Hawaiian Islands. This observation also aligns with the unconfined nature of the extensive freshwater Biscayne aquifer in the region (Cunningham & Florea, 2009). However, attributing the observed resistivity spikes solely to sources of fresh SGD is problematic because bulk resistivity reflects both water chemistry and the petrophysical properties of the surrounding environment (Manheim et al., 2004). I did not detect fresh SGD in any groundwater endmembers collected from anomaly areas (Table 3.0). Furthermore, the statistical analysis (section 3.6) suggested that there are negligible differences in salinity and radon levels between the anomaly areas (“A” zones) and the background (“N” zones). I therefore propose that the anomalous spike in resistivity originate from factors other than variations in groundwater chemistry. The upwelling anomalies observed ER profiles (see Fig. 4.2) are not primarily influenced by changes in groundwater salinity but instead by variations in subsurface lithology, porosity, or saturation. Zamrsky et al. (2020) reported that geological heterogeneity can significantly influence ER measurements, leading to anomalies that do not correspond to variations in groundwater chemistry. The spikes might indicate the presence of vuggy porosity and cavities within seabeds (Juster et al., 1997). Cunningham et al. (2004) demonstrated the prevalence of vuggy porosity and karstic structures in the Biscayne aquifer, which is a part of the aquifer system in the Miami Limestone underlying the bay. Typically, karstic structures increase porosity due to fractures, which results in a significant reduction in resistivity values, mimicking the resistivity of seawater (Barcaglioni et al., 2021). However, the encroachment of carbonate muds and seawater into the collapse structures increases the resistivity

of the karst formations, contrasting sharply with the hypersaline groundwater in the vicinity. This pattern is observed in the ER profile (Fig. 4.2; right panel).

The recirculated seawater causes minimal variance in bulk resistivity observed in Florida Bay and presents a significant challenge for using the ERT method in detecting SGD within the region. Since the ER method relies on identifying variations in dissolved ions in marine environments to detect SGD signals (Johnson et al., 2015), the negligible variance in resistivity hinders the ability of ER to distinguish SGD signals effectively. Despite this challenge, the dipole-dipole array configuration, owing to its high signal-to-noise ratio in marine environments (Rucker et al., 2011), allowed for the identification of spikes in the ER profile and pockets of hypersaline groundwater (Fig. 4.2; left panel). The limitation of the ER could result from a potential balanced exchange of water across the sediment/water interface. The discharge of hypersaline groundwater into Florida Bay may be counteracted by the influx of seawater into the underlying aquifer. This dynamic equilibrium can result in a net zero exchange of water across the sediment/water interface, effectively masking SGD into the bay as detected by ER methods. Hypersaline groundwater is denser than the saline surface seawater and could discharge into the surface driven by buoyancy and density-driven flow. Hypersaline groundwater, being denser than the overlying seawater, acts like a heavy fluid. This density difference creates a natural buoyancy force that can push the denser groundwater upwards. This upward movement, driven by density gradients, could lead to the discharge of hypersaline groundwater into the surface water of the bay (van Engelen et al., 2018). Tides, even small ones like microtides, can play a significant role in this process. As tides rise and fall, they can act like a pump, squeezing and releasing groundwater through the seabed (Chanton et al., 2003). This "pumping" action could facilitate the discharge of hypersaline groundwater into the bay. Chanton et al. (2003) explained that Atlantic tidal pumping cause saline water to oscillate into the groundwater system. They opined that once seawater enters the aquifer, it becomes

groundwater, though it originally came from the sea. Recirculated seawater likely reaches only the upper few meters of the limestone (Chanton et al., 2003). Hence, tidal pumping within the Miami Limestone likely leads to the mixing and dispersion of existing water, rather than significant advection of seawater, influencing the depth to which recirculated seawater penetrates the limestone member (Reich et al., 2002).

In wavy conditions, the vertical oscillation of electrodes can disrupt their contact with the water surface, compromising measurement accuracy. Some datasets obtained from Rankin and Whipray Basins experienced high noise levels which rendered them unusable for the inversion. According to Thompson et al. (2012), such errors could arise from poor electrode contact and increased wave action in shallow water. The shallower depth (less than 1 meter) in Rankin Basin could have contributed to this. As the boat navigates against wind and waves, boat engine noise, particularly in shallow water where it might be more prominent, can act as an electrical source that interferes with the actual resistivity measurements (Binley et al., 1995). Moreover, I encountered measurement device errors as the SuperSting intermittently shut down during data acquisition. I observed that the SuperSting requires controlled temperatures and often shuts off in the 30-degree Celsius conditions of Florida Bay.

4.2 Statistical Interpretation of Groundwater Samples

The primary objective of the statistical analyses was to determine if the distribution of salinity and radon activity in the identified anomalous zones ("A") significantly differ from those in the background ("N") dataset. Identifying significant differences in these distributions is crucial to ascertain whether the observed anomalies primarily stem from variations in groundwater chemistry (Dzakpasu et al., 2014). At a significance level of $\alpha = 0.05$, the statistical tests for mean salinity patterns in the Rankin, Whipray, and Rabbit Key Basins revealed that any observed differences in groundwater salinity levels between the anomaly and background zones within these

basins are not statistically significant. This implies that salinity in these basins exhibit spatial uniformity. Interestingly, the groundwater salinity in these basins mirror similar patterns of spatial homogeneity of the surface salinity. Kelble et al. (2007) noted that the greater inter-basin water exchange in Whipray Basin leads to less variable seawater salinity. Essentially, the groundwater salinity variations within and across these basins are consistent, and any minor differences are likely due to other factors rather than groundwater salinity. Moreover, there was no significant deviation in groundwater salinity, aggregated across the whole basin, in the anomaly and normal zones. This emphasizes regional spatial homogeneity of salinity in the anomaly and normal zones across Florida Bay.

Our analysis showed that radon activity in the "A" (anomalous) and "N" (normal) zones did not differ significantly across any of the three basins. Radon-222 distribution serves as a proxy for estimating the apparent volume of SGD and groundwater residence times (Kelly et al., 2018). Interestingly, I observed both high and low radon activity, indicating areas of high and low SGD respectively, across the basins. Statistical analysis (Table 3.2) strongly indicated that radon activity did not align with the anomalous or background categories derived from the ER profiles. The radon activity in the "A" and "N" zones were non-unique, suggesting that radon activity in groundwater is spatially similar between these zones. Moreso, the pooled mean radon activity across entire basins showed no significant difference between the "A" and "N" regions. This indicates that, at both local and regional scales, radon activity in groundwater endmembers in Florida Bay is not confined to the predefined anomalous or normal categories.

The variations in salinity and radon activity in the anomalous zones are not substantial enough to contrast with the background dataset, thus supporting our hypothesis that the anomalies observed in the "A" zones stem from the petrophysical properties of the underlying formation rather than the water chemistry. Since radon activity do not vary significantly in the anomalous

zones, the roles of the karstic feature as SGD pathways appears similar to that of surrounding regions. This supports our hypothesis that collapsed karst structures are infilled with mud, which lowers permeability and influences the dynamics of SGD.

As observed from Table 3.0, there is an average deviation of 4.9 m ($n = 15$) between the locations where groundwater endmembers were collected, and the target locations derived from the ER profiles. Perhaps, this deviation from the target location impacted the accuracy of the hydrochemical parameters. The SGD recorded across the study area is not characterized by discrete freshwater springs but rather occurs through diffuse seepage over a few meters. Consequently, the data obtained from the anomalous ("A") zones might be mixed with the background data due to the imprecise positioning of the boat during sampling. Due to buoyancy and wave action during boat survey, it is difficult to pinpoint the exact target locations I derived from the ER profile. In the ER profile, the average anomaly zone occurs in a range of 0.3 m to about 2.5 m, and I targeted these zones during discrete in-situ sampling. However, with an average location difference of 4.9 m, the fluctuating positioning of the boat made it problematic to grab groundwater endmembers at the exact target observed from the ER. To achieve more accurate sampling of the "A" zones, a technique with greater GPS precision, such as scuba diving (e.g. Kamermans et al., 2002) and underwater spectrometer (e.g.; Eleftheriou et al., 2020), could be employed. This might yield statistical results that deviate from those I reported, and potentially provide a clearer distinction in the hydrochemical characteristics between the anomalous and normal zones.

4.3 Groundwater End Members

I did not detect freshwater springs in the basins, which was corroborated by the hypersalinity of the groundwater endmembers (Table 3.0). Corbett et al. (1999) documented that most groundwater samples from shallow wells in Florida Bay are saline to hypersaline. The salinity

levels of the groundwater endmembers were well above the typical seawater salinity range of 33-37 ppt (National Oceanic and Atmospheric Administration, 2023a). The elevated groundwater salinity readings are consistent with previous studies, indicating a persistent temporal trend in the region. For example, Burns and Swart (1992) reported hypersaline pore waters beneath the bay's central area, surpassing surface seawater salinity. As observed from the ER profile, the SGD in Florida Bay primarily consists of recirculated seawater, with no discernible input from fresh water sources, aligning with the findings of Swarzenski et al. (2009) and Corbett et al. (2000). Also, Swart and Kramer (2004) noted that groundwater on nearby islands tends to be hypersaline, with total dissolved solids nearing 150 parts per thousand (ppt). Furthermore, Swart et al. (1989) reported even more pronounced salinity in pore water on these islands. Their study found pore water salinity to be 2-3 times greater than surface seawater salinity in the bay. This historical pattern of hypersalinity indicates that groundwater endmembers remain elevated over time, both within the bays and surrounding islands.

While high evaporation rates and minimal freshwater input contribute to elevated salinity in Florida Bay's surface water (Kelble et al., 2007), the factors driving hypersalinity in the groundwater endmembers remain unclear. Juster et al. (1997) proposed a mechanism involving density inversion caused by the bay's unique sedimentary composition. Their hypothesis centers on the presence of low-permeability muddy sediments with a hydraulic conductivity approximately $10^{-2.5}$ m per day⁻¹. This characteristic of the Miami Oolite formation significantly restricts water movement within the basins (Juster et al., 1997). Consequently, the low interstitial velocities trap saline surface water within the basin interiors (Juster et al., 1997). As evaporation concentrates salts in the surface water (Price et al., 2007), these denser brines sink due to their increased density and potentially contribute to the salinity of the underlying groundwater. Lee et al. (2006) argued that seawater hypersalinity in the bay stems from the lack of freshwater input

from the Everglades, limited interaction with the open sea, restricted water exchange between basins, and prolonged residence time. I propose that during periods of increased precipitation or freshwater inflow, such as floods or water management practices, denser, saltier seawater infiltrates the subsurface, thereby increasing salinity in groundwater endmembers. The hypersaline groundwater endmembers, which showed higher salinity than surface seawater, suggests subsurface interactions with geological materials that increased salinity of recirculated seawater. However, given that the composition of the Miami Limestone comprises biogenic aragonite (50-60%) and calcite (30-40%) (Jensen et al., 2009), the source of saliferous materials in the subsurface remains unclear. Fresh discharge, if any, has minimal impact on the salinity of groundwater endmembers in Florida Bay (Corbett et al., 1999).

The remarkable hypersalinity (up to 45 ppt) observed in groundwater from Rankin Basin is concerning, as salinity exceeding 40 ppt are considered detrimental to the bay's ecosystem (Stabenau & Kotun, 2012). As highlighted by Murray et al. (2010), Rankin Basin's geographical features, characterized by shallow carbonate mud banks surrounded by mangrove islands, act as barriers to tidal mixing and mitigate the influence of tides and currents (Boyer et al., 1999). SGD flow in Rankin is influenced more by topography than tidal pumping (Corbett et al., 2000). This geography potentially contributes to the development of hypersaline conditions in the bay. Notably, during the drought of 1989-90, Rankin Basin experienced exceptionally high salinity (Murray et al., 2010). During this period, Fourqurean et al. (1992) documented extreme high salinity within the basin, exceeding 50 ppt. This extreme salinity event underscores the vulnerability of Rankin Basin to environmental fluctuations and highlights the potential consequences of its geographical constraints. Considering that the salinity data reported here were measured in January, the elevated salinity of the bay is higher than the January data recorded by Kelble et al. (2007), which suggested a change in the salinity pattern over the years. However,

Kelble et al. (2007) documented the dramatic changes in the bay's salinity which can change more than 0.5 ppt per day, either elevating or decreasing. The higher salinity in Rankin Basin and Whipray Basin agrees with the historic higher salinity in the northwestern and central part of the bay, which experienced more severe seagrass die-off (Jensen et al., 2009; Kelbe et al., 2007; Lee et al., 2006; Robbins, 2023).

4.4 Broader Implications

The changing hydrology and ecology of Florida Bay sparked scientific and management concerns across different scales. Among these concerns, water quality stands as the most critical. In addition to the Comprehensive Everglades Restoration Plan (CERP), the US Environmental Protection Agency (EPA), the State of Florida, and other agencies continue to invest billions of dollars to enhance water quality in the lower Everglades (Stainback et al., 2020). According to Stabenau and Kotun (2012), the CERP program identified salinity as a key restoration performance measure for Florida Bay, with guidelines established to: (1) reduce the occurrence of hypersaline events annually, (2) increase the frequency and spatial extent of lower salinity conditions, and (3) ensure more stable water conditions by preventing rapid decreases in salinity in the northeastern region of the bay. With this strategy in mind, recent initiatives by the Florida Bay management have focused on continuous monitoring of salinity to address areas of sustained hypersalinity by supplying freshwater to the bay. The newly implemented Florida Bay Improvement Project in the upper Taylor Slough area is expected to enhance freshwater flows in both the southern Everglades and Florida Bay (South Florida Water Management District, 2018). In this study, I observed relatively lower and consistent groundwater salinity values in Whipray Basin and Rabbit Key Basin compared to Rankin Basin. This suggests that Whipray and Rabbit Key Basins offer a more stable environment for marine life, potentially fostering higher biodiversity and ecological resilience. The hypersalinity observed in groundwater from Rankin Basin highlights its

vulnerability to environmental fluctuations, necessitating enhanced monitoring and effective water management practices. The persistent hypersalinity in Florida Bay has been associated with various ecosystem disruptions (Hall et al., 2016; Lee et al., 2006; Nuttle et al., 2000; Zieman et al., 1999). I have further examined the input of even more hypersaline conditions in the subsurface.

The persistence of hypersaline groundwater, as indicated by elevated salinity in groundwater endmembers, has significant implications for the bay's overall hydrology and water quality. Understanding groundwater chemistry is crucial for implementing effective water management practices to sustain the bay's ecology. It informs strategies to preserve water quality and mitigate the impacts of hypersalinity on marine ecosystems. The driving force behind the hypersalinity across the basin remains unclear. Potential explanations include density inversion caused by the bay's unique sediments, interaction with saline geological formations, and limited freshwater recharge leading to evaporation (Juster et al., 1997). Furthermore, the geographical features of Rankin Basin, such as shallower carbonate mud banks and mangrove islands, contribute to the development of hypersaline conditions compared to Whipray and Rabbit Key Basins. This highlights the interconnectedness between geomorphological features and hydrological processes, emphasizing the need for integrated coastal management approaches that consider both natural and anthropogenic influences.

I likely delineated karstic structures and their complex roles in groundwater dynamics within Florida Bay. The identification of collapsed cavities and vugs filled with carbonate muds is crucial for advancing our understanding of the sedimentology and structural geology of Florida Bay. Rodemann et al. (2021) highlighted that suspended sediments influences seagrass health, suggesting that the presence of karstic features and sediments infilling them could potentially impact ecosystem dynamics in the bay. These findings show the importance of integrating karstic influences into ecosystem monitoring within the bay.

4.5 Limitations and Future Steps

The ERT method used to detect SGD has limitations in Florida Bay, which is dominated by recirculated seawater. A balanced exchange of seawater into the aquifer and hypersaline groundwater discharge out of it could create a net zero flux, masking the signals of SGD in the ER readings. More sophisticated methods to detect and quantify SGD are crucial for creating a more complete picture of water exchange dynamics in the bay. With minimal resistivity variance in the ERT profile, only small pockets of hypersaline SGD were identified, with no fresh SGD detected. Therefore, deploying additional sensors or tracers is necessary for a more comprehensive understanding and accurate mapping of these discharge zones.

Further research is needed to pinpoint the exact mechanisms driving hypersalinity in the groundwater. This could involve studies on factors like the bay's unique sediment composition, interaction with underlying geological formations, and the role of freshwater recharge limitations. Investigating the ecological consequences of hypersaline groundwater discharge on the various organisms and ecosystems within Florida Bay is vital. This will help understand how salinity fluctuations affect the bay's delicate balance. Measuring the volume of hypersaline groundwater entering the bay is essential to understand its overall impact on salinity in the bay. This could involve techniques like hydrogeological modeling or isotope studies.

The impact of SAV on ER is not well defined. Future research can conduct focused ER surveys within seagrass meadows to isolate the impact of seagrass on the overall resistivity signal. By comparing these measurements to areas without seagrass, scientists can differentiate the influence of the meadows from the underlying geological composition. Moreover, developing and refining ER models that incorporate the unique characteristics of seagrass meadows is crucial. These models should account for the variable water content within the seagrass tissues, the root structure that creates channels and voids, and the potential bioelectrical activity of the meadows.

4.6 Conclusion

The characterization of subterranean flow in Florida Bay through salinity measurements, radon activity analysis, and geophysical anomalies sheds light on the interaction of hydrological processes and geological factors shaping this unique coastal ecosystem. Through the integration of in situ hydrochemical measurements, ER surveys, and statistical analyses, I have gained valuable insights on the composition of SGD in the bay, as well as salinity variations of the groundwater, which have implications for both management strategies and scientific research.

The identification of anomalous resistivity spikes in ERT profiles set the pace for the characterization of SGD within Florida Bay. Despite initial associations between elevated resistivity zones and potential freshwater ingress, the complexities of the bay's environmental conditions underscore the need for cautious interpretation. Through in-situ measurement of salinity and radon-222 activities, I hypothesize that geological heterogeneity, subsurface lithology, and porosity variations are the primary factors influencing geophysical anomalies, complicating straightforward correlation with groundwater chemistry. I did not delineate freshwater springs from the ER profile, and the groundwater endmembers were hypersaline, supporting the conclusion that SGD in the bay consisted of recirculated seawater.

Moreover, our statistical interpretation of groundwater samples indicates spatial homogeneity in salinity patterns and radon activity across the basins of Florida Bay, showing no significant influence from the various karstic features present. These findings show the nature of hydrological dynamics within the bay, influenced by basin morphology, inter-basin water exchange, and regional marine influences.

From a management perspective, our findings highlight the importance of holistic approaches to water resource management in Florida Bay. Prioritizing stable habitats for conservation efforts, mitigating the impacts of salinity stress on sensitive species, and integrating

interdisciplinary research into management strategies are essential steps towards preserving the ecological health and resilience of the bay. Furthermore, our study highlights the need for innovative approaches to SGD detection and quantification in coastal environments. Integrating advanced geophysical techniques, hydrological modeling, and field observations can enhance our understanding of groundwater dynamics and their ecological implications.

I discovered various locations of saline SGD spatially distributed across the bay. From the ERT data, there is no significant difference between the SGD in wet and dry seasons and this is influenced by the low freshwater input, no extreme events recorded in the bay within the period under study (2021 to 2024), and minimal influence of surficial processes on the subsurface processes. I delineated varying karstic structures of width and depth in the ERT profiles. These structures exhibited a broader range of resistivity ranges and varying groundwater flow pattern. Also, these karstic structures do not differ between wet and dry seasons. We noted that the key environmental factors influencing variations of SGD in the bay are topographical setting, especially in Rankin (Murray et al., 2010), microtidal and hydrodynamic processes (Corbett et al., 2000), climate variability and sea level rise (Dessu et al., 2018), sediment characteristics and karstic structures.

In summary, this research highlights the complex and dynamic nature of Florida Bay's hydrological system, emphasizing the importance of interdisciplinary research and collaborative management efforts. By bridging the gap between scientific inquiry and management action, we can work towards sustainable conservation and stewardship of this invaluable coastal ecosystem.

REFERENCES

Advanced Geosciences (2009). Instruction manual for EarthImager 2D resistivity and IP inversion software.

<https://geophysicalequipmentrental.com/files/2020/01/EarthImager2DManual.pdf>

Adyasari, D., Hassenrück, C., Montiel, D., & Dimova, N. (2020). Microbial community composition across a coastal hydrological system affected by submarine groundwater discharge (SGD). *PLOS ONE*, *15*(6).

<https://doi.org/10.1371/journal.pone.0235235>

Adyasari, D., Montiel, D., Mortazavi, B., & Dimova, N. (2021). Storm-Driven Fresh Submarine Groundwater Discharge and Nutrient Fluxes from a Barrier Island.

Frontiers in Marine Science, *8*, 679010. <https://doi.org/10.3389/fmars.2021.679010>

Amato, M., Basso, B., Celano, G., Bitella, G., Morelli, G., & Rossi, R. (2008). In situ detection of tree root distribution and biomass by multi-electrode resistivity imaging. *Tree Physiology*, *28*(10), 1441–1448.

<https://doi.org/10.1093/treephys/28.10.1441>

Amato, M., Rossi, R., Bitella, G., & Lovelli, S. (2010). Multielectrode Geoelectrical Tomography for the Quantification of Plant Roots. *Italian Journal of Agronomy*, *5*(3), 257. <https://doi.org/10.4081/ija.2010.257>

Arboleda-Zapata, M., Angelopoulos, M., Overduin, P. P., Grosse, G., Jones, B. M., & Tronicke, J. (2022). Exploring the capabilities of electrical resistivity tomography to study subsea permafrost. *The Cryosphere*, *16*(10), 4423–4445.

<https://doi.org/10.5194/tc-16-4423-2022>

Archie, G. E. (1942). The Electrical Resistivity Log as an Aid in Determining Some Reservoir Characteristics. *Transactions of the AIME*, 146(01), 54–62.

<https://doi.org/10.2118/942054-G>

Athanasίου, E. N., Tsourlos, P. I., Papazachos, C. B., & Tsokas, G. N. (2009). Optimizing Electrical Resistivity Array Configurations by Using a Method Based on the Sensitivity Matrix. *Near Surface 2009 - 15th EAGE European Meeting of Environmental and Engineering Geophysics*. Near Surface 2009 - 15th EAGE European Meeting of Environmental and Engineering Geophysics, Dublin, Ireland.

<https://doi.org/10.3997/2214-4609.20147025>

Attias, E., Constable, S., Sherman, D., Ismail, K., Shuler, C., & Dulai, H. (2021). Marine Electromagnetic Imaging and Volumetric Estimation of Freshwater Plumes Offshore Hawai'i. *Geophysical Research Letters*, 48(7), e2020GL091249.

<https://doi.org/10.1029/2020GL091249>

Attias, E., Thomas, D., Sherman, D., Ismail, K., & Constable, S. (2020). Marine electrical imaging reveals novel freshwater transport mechanism in Hawai'i. *Science Advances*, 6(48), eabd4866. <https://doi.org/10.1126/sciadv.abd4866>

Banda, K., Ngwenya, V., Mulema, M., Chomba, I., Chomba, M., & Nyambe, I. (2023). Influence of water quality on benthic macroinvertebrates in a groundwater-dependent wetland. *Frontiers in Water*, 5, 1177724.

<https://doi.org/10.3389/frwa.2023.1177724>

Barcaglioni, V., Canna, G., Vecchio, G., Ponte, M., & Ferraro, G. (2021). *Geophysical Survey on the Offshore Microtunnel Route in Delimara Peninsula (MALTA)*. OMC Med Energy Conference and Exhibition. <https://dx.doi.org/>

- Binley, A., Ramirez, A., & Daily, W. (1995). Regularised Image Reconstruction of Noisy Electrical Resistance Tomography Data. *Process Tomography*, 401–410.
- Black, F. J., Paytan, A., Knee, K. L., De Sieyes, N. R., Ganguli, P. M., Gray, E., & Flegal, A. R. (2009). Submarine Groundwater Discharge of Total Mercury and Methylmercury to Central California Coastal Waters. *Environmental Science & Technology*, 43(15), 5652–5659. <https://doi.org/10.1021/es900539c>
- Blake, E. S., Landsea, C., & Gibney, E. J. (2007). *The deadliest, costliest, and most intense United States tropical cyclones from 1851 to 2010*. <https://repository.library.noaa.gov/view/noaa/6929>
- Boyer, J. N., Fourqurean, J. W., & Jones, R. D. (1999). Seasonal and long-term trends in the water quality of Florida Bay (1989–1997). *Estuaries*, 22(2), 417–430. <https://doi.org/10.2307/1353208>
- Branchet, P., Arpin-Pont, L., Piram, A., Boissery, P., Wong-Wah-Chung, P., & Doumenq, P. (2021). Pharmaceuticals in the marine environment: What are the present challenges in their monitoring? *Science of The Total Environment*, 766, 142644. <https://doi.org/10.1016/j.scitotenv.2020.142644>
- Burnett, W. C., Aggarwal, P. K., Aureli, A., Bokuniewicz, H., Cable, J. E., Charette, M. A., Kontar, E., Krupa, S., Kulkarni, K. M., Loveless, A., Moore, W. S., Oberdorfer, J. A., Oliveira, J., Ozyurt, N., Povinec, P., Privitera, A. M. G., Rajar, R., Ramessur, R. T., Scholten, J., ... Turner, J. V. (2006). Quantifying submarine groundwater discharge in the coastal zone via multiple methods. *Science of The Total Environment*, 367(2–3), 498–543. <https://doi.org/10.1016/j.scitotenv.2006.05.009>

- Burnett, W. C., Bokuniewicz, H., Huettel, M., Moore, W. S., & Taniguchi, M. (2003). Groundwater and pore water inputs to the coastal zone. *Biogeochemistry*, 66(1), 3–33. <https://doi.org/10.1023/B:BIOG.0000006066.21240.53>
- Burnett, W. C., & Dulaiova, H. (2003). Estimating the dynamics of groundwater input into the coastal zone via continuous radon-222 measurements. *Journal of Environmental Radioactivity*, 69(1–2), 21–35. [https://doi.org/10.1016/S0265-931X\(03\)00084-5](https://doi.org/10.1016/S0265-931X(03)00084-5)
- Burns, S. J., & Swart, P. K. (1992). Diagenetic processes in Holocene carbonate sediments: Florida Bay mudbanks and islands. *Sedimentology*, 39(2), 285–304. <https://doi.org/10.1111/j.1365-3091.1992.tb01039.x>
- Cardenas, M. B., Zamora, P. B., Siringan, F. P., Lapus, M. R., Rodolfo, R. S., Jacinto, G. S., San Diego-McGlone, M. L., Villanoy, C. L., Cabrera, O., & Senal, M. I. (2010). Linking regional sources and pathways for submarine groundwater discharge at a reef by electrical resistivity tomography, ²²²Rn, and salinity measurements. *Geophysical Research Letters*, 37(16), 2010GL044066. <https://doi.org/10.1029/2010GL044066>
- Carlson, D. F., Yarbrow, L. A., Scolaro, S., Poniatowski, M., McGee-Absten, V., & Carlson, P. R. (2018). Sea surface temperatures and seagrass mortality in Florida Bay: Spatial and temporal patterns discerned from MODIS and AVHRR data. *Remote Sensing of Environment*, 208, 171–188. <https://doi.org/10.1016/j.rse.2018.02.014>
- Carlson, P., Yarbrow, L. A., & Barber, T. R. (1994). Relationship of Sediment Sulfide to Mortality of *Thalassia Testudinum* in Florida Bay. *Bulletin of Marine Science*, 54(3), 733–746.

- Chanton, J. P., Burnett, W. C., Dulaiova, H., Corbett, D. R., & Taniguchi, M. (2003). Seepage Rate Variability in Florida Bay Driven by Atlantic Tidal Height. *Biogeochemistry*, *66*(1/2), 187–202. <https://www.jstor.org/stable/1469889>
- Corbett, D. R., Chanton, J., Burnett, W., Dillon, K., Rutkowski, C., & Fourqurean, J. W. (1999). Patterns of groundwater discharge into Florida Bay. *Limnology and Oceanography*, *44*(4), 1045–1055. <https://doi.org/10.4319/lo.1999.44.4.1045>
- Corbett, D. R., Dillon, K., Burnett, W., & Chanton, J. (2000). Estimating the groundwater contribution into Florida Bay via natural tracers, ^{222}Rn and CH_4 . *Limnology and Oceanography*, *45*(7), 1546–1557. <https://doi.org/10.4319/lo.2000.45.7.1546>
- Cross, V. A., Bratton, J. F., Michael, H. A., Kroeger, K. D., Mann, A. G., & Bergeron, E. M. (2011). *Continuous resistivity profiling and seismic-reflection data collected in April 2010 from Indian River Bay, Delaware* (Nos. 2011–1039). U.S. Geological Survey. <https://doi.org/10.3133/ofr20111039>
- Cunningham, K., & Florea, L. (2009). The Biscayne Aquifer of Southeastern Florida. *Caves and Karst of America*, 2009, 196–199. https://digitalcommons.wku.edu/geog_fac_pub/20
- Cunningham, K. J., Carlson, J. I., & Hurley, N. F. (2004). New method for quantification of vuggy porosity from digital optical borehole images as applied to the karstic Pleistocene limestone of the Biscayne aquifer, southeastern Florida. *Journal of Applied Geophysics*, *55*(1–2), 77–90. <https://doi.org/10.1016/j.jappgeo.2003.06.006>
- Dessu, S. B., Price, R. M., Troxler, T. G., & Kominoski, J. S. (2018). Effects of sea-level rise and freshwater management on long-term water levels and water quality in the Florida Coastal Everglades. *Journal of Environmental Management*, *211*, 164–176. <https://doi.org/10.1016/j.jenvman.2018.01.025>

- Dimova, N. T., Swarzenski, P. W., Dulaiova, H., & Glenn, C. R. (2012). Utilizing multichannel electrical resistivity methods to examine the dynamics of the fresh water–seawater interface in two Hawaiian groundwater systems. *Journal of Geophysical Research: Oceans*, *117*(C2), 2011JC007509.
<https://doi.org/10.1029/2011JC007509>
- Dzakpasu, M., Scholz, M., Harrington, R., McCarthy, V., & Jordan, S. (2014). Groundwater Quality Impacts from a Full-Scale Integrated Constructed Wetland. *Groundwater Monitoring & Remediation*, *34*(3), 51–64.
<https://doi.org/10.1111/gwmr.12059>
- Ehlert Von Ahn, C. M., Dellwig, O., Szymczycha, B., Kotwicki, L., Rooze, J., Endler, R., Escher, P., Schmiedinger, I., Sültenfuß, J., Diak, M., Gehre, M., Struck, U., Vogler, S., & Böttcher, M. E. (2024). Submarine groundwater discharge into a semi-enclosed coastal bay of the southern Baltic Sea: A multi-method approach. *Oceanologia*, *66*(1), 111–138. <https://doi.org/10.1016/j.oceano.2024.01.001>
- Eleftheriou, G., Pappa, F. K., Maragos, N., & Tsabaris, C. (2020). Continuous monitoring of multiple submarine springs by means of gamma-ray spectrometry. *Journal of Environmental Radioactivity*, *216*, 106180.
<https://doi.org/10.1016/j.jenvrad.2020.106180>
- Enos, P., & Perkins, R. D. (1979). Evolution of Florida Bay from island stratigraphy. *Geological Society of America Bulletin*, *90*(1), 59. [https://doi.org/10.1130/0016-7606\(1979\)90<59:EOFBFI>2.0.CO;2](https://doi.org/10.1130/0016-7606(1979)90<59:EOFBFI>2.0.CO;2)
- Enos, P., & Sawatsky, L. H. (1981). Pore Networks in Holocene Carbonate Sediments. *SEPM Journal of Sedimentary Research*, *51*. <https://doi.org/10.1306/212F7DF1-2B24-11D7-8648000102C1865D>

- Fish, J. E., & Stewart, M. T. (1991). *Hydrogeology of the surficial aquifer system, Dade County, Florida*. <https://doi.org/10.3133/wri904108>
- Florida Fish and Wildlife Conservation Commission. (2023). *Coral Bleaching*. Florida Fish and Wildlife Conservation Commission. <https://myfwc.com/research/habitat/coral/news-information/bleaching/>
- Fourqurean, J. W., & Robblee, M. B. (1999). Florida Bay: A history of recent ecological changes. *Estuaries*, 22(2), 345–357. <https://doi.org/10.2307/1353203>
- Fourqurean, J. W., Zieman, J. C., & Powell, G. V. N. (1992). Phosphorus limitation of primary production in Florida Bay: Evidence from C:N:P ratios of the dominant seagrass *Thalassia testudinum*. *Limnology and Oceanography*, 37(1), 162–171. <https://doi.org/10.4319/lo.1992.37.1.0162>
- Fredley, J., Durako, M. J., & Hall, M. O. (2019). Multivariate analyses link macrophyte and water quality indicators to seagrass die-off in Florida Bay. *Ecological Indicators*, 101, 692–701. <https://doi.org/10.1016/j.ecolind.2019.01.074>
- Fu, T., Zhang, Y., Xu, X., Qiao Su, Chen, G., & Guo, X. (2020). Assessment of submarine groundwater discharge in the intertidal zone of Laizhou Bay, China, using electrical resistivity tomography. *Estuarine, Coastal and Shelf Science*, 245, 106972. <https://doi.org/10.1016/j.ecss.2020.106972>
- Garcia-Orellana, J., Rodellas, V., Tamborski, J., Diego-Feliu, M., Van Beek, P., Weinstein, Y., Charette, M., Alorda-Kleinglass, A., Michael, H. A., Stieglitz, T., & Scholten, J. (2021). Radium isotopes as submarine groundwater discharge (SGD) tracers: Review and recommendations. *Earth-Science Reviews*, 220, 103681. <https://doi.org/10.1016/j.earscirev.2021.103681>

- Gerlach, M. E., Rains, K. C., Guerrón-Orejuela, E. J., Kleindl, W. J., Downs, J., Landry, S. M., & Rains, M. C. (2021). Using Remote Sensing and Machine Learning to Locate Groundwater Discharge to Salmon-Bearing Streams. *Remote Sensing*, *14*(1), 63. <https://doi.org/10.3390/rs14010063>
- Griffiths, D. H., & Barker, R. D. (1993). Two-dimensional resistivity imaging and modelling in areas of complex geology. *Journal of Applied Geophysics*, *29*(3), 211–226. [https://doi.org/10.1016/0926-9851\(93\)90005-J](https://doi.org/10.1016/0926-9851(93)90005-J)
- Hagedorn, B., & Tsuda, M. (2022). Radon and Salinity Mass Balance Constraints on Groundwater Recharge on a Semi-Arid Island (Catalina, California). *Water*, *14*(7), 1068. <https://doi.org/10.3390/w14071068>
- Hall, M., Furman, B., Merello, M., & Durako, M. (2016). Recurrence of *Thalassia testudinum* seagrass die-off in Florida Bay, USA: initial observations. *Marine Ecology Progress Series*, *560*, 243–249. <https://doi.org/10.3354/meps11923>
- Halley, R. B., Vacher, H. L., & Shinn, E. A. (2004). Geology and Hydrogeology of the Florida Keys. In *Developments in Sedimentology*, *54*, 217–248. Elsevier. [https://doi.org/10.1016/S0070-4571\(04\)80027-X](https://doi.org/10.1016/S0070-4571(04)80027-X)
- Hermans, T., & Paepen, M. (2020). Combined Inversion of Land and Marine Electrical Resistivity Tomography for Submarine Groundwater Discharge and Saltwater Intrusion Characterization. *Geophysical Research Letters*, *47*(3), e2019GL085877. <https://doi.org/10.1029/2019GL085877>
- Jackson, P. D., Briggs, K. B., Flint, R. C., Holyer, R. J., & Sandidge, J. C. (2002). Two- and three-dimensional heterogeneity in carbonate sediments using resistivity imaging. *Marine Geology*, *182*(1–2), 55–76. [https://doi.org/10.1016/S0025-3227\(01\)00228-6](https://doi.org/10.1016/S0025-3227(01)00228-6)

- Jensen, H. S., Nielsen, O. I., Koch, M. S., & De Vicente, I. (2009). Phosphorus release with carbonate dissolution coupled to sulfide oxidation in Florida Bay seagrass sediments. *Limnology and Oceanography*, *54*(5), 1753–1764.
<https://doi.org/10.4319/lo.2009.54.5.1753>
- Jobbágy, V., Stroh, H., Marissens, G., & Hult, M. (2019). Comprehensive study on the technical aspects of sampling, transporting and measuring radon-in-water. *Journal of Environmental Radioactivity*, *197*, 30–38. <https://doi.org/10.1016/j.jenvrad.2018.11.012>
- Johnson, C. D., Swarzenski, P. W., Richardson, C. M., Smith, C. G., Kroeger, K. D., & Ganguli, P. M. (2015). Ground-truthing Electrical Resistivity Methods in Support of Submarine Groundwater Discharge Studies: Examples from Hawaii, Washington, and California. *Journal of Environmental and Engineering Geophysics*, *20*(1), 81–87. <https://doi.org/10.2113/JEEG20.1.81>
- Jou-Claus, S., Folch, A., & Garcia-Orellana, J. (2021). Applicability of Landsat 8 thermal infrared sensor for identifying submarine groundwater discharge springs in the Mediterranean Sea basin. *Hydrology and Earth System Sciences*, *25*(9), 4789–4805.
<https://doi.org/10.5194/hess-25-4789-2021>
- Juster, T., Kramer, P. A., Vacher, H. L., Swart, P. K., & Stewart, M. (1997). Groundwater flow beneath a hypersaline pond, Cluett Key, Florida Bay, Florida. *Journal of Hydrology*, *197*(1–4), 339–369. [https://doi.org/10.1016/S0022-1694\(96\)03103-4](https://doi.org/10.1016/S0022-1694(96)03103-4)
- Kamermans, P., Hemminga, M., Tack, J., Mateo, M., Marbà, N., Mtolera, M., Stapel, J., & Verheyden, A. (2002). Groundwater effects on diversity and abundance of lagoonal seagrasses in Kenya and on Zanzibar Island (East Africa). *Marine Ecology Progress Series*, *231*, 75–83. <https://doi.org/10.3354/meps231075>

- Kelble, C. R., Johns, E. M., Nuttle, W. K., Lee, T. N., Smith, R. H., & Ortner, P. B. (2007). Salinity patterns of Florida Bay. *Estuarine, Coastal and Shelf Science*, *71*(1–2), 318–334. <https://doi.org/10.1016/j.ecss.2006.08.006>
- Kelly, J. L., Dulai, H., Glenn, C. R., & Lucey, P. G. (2018). Integration of aerial infrared thermography and in situ radon-222 to investigate submarine groundwater discharge to Pearl Harbor, Hawaii, USA. *Limnology and Oceanography*, *64*(1), 238–257. <https://doi.org/10.1002/lno.11033>
- Kelly, J. L., Glenn, C. R., & Lucey, P. G. (2013). High-resolution aerial infrared mapping of groundwater discharge to the coastal ocean. *Limnology and Oceanography: Methods*, *11*(5), 262–277. <https://doi.org/10.4319/lom.2013.11.262>
- Koch, M. S., Schopmeyer, S. A., Nielsen, O. I., Kyhn-Hansen, C., & Madden, C. J. (2007). Conceptual model of seagrass die-off in Florida Bay: Links to biogeochemical processes. *Journal of Experimental Marine Biology and Ecology*, *350*(1–2), 73–88. <https://doi.org/10.1016/j.jembe.2007.05.031>
- Lagomasino, D., Fatoyinbo, T., Castañeda-Moya, E., Cook, B. D., Montesano, P. M., Neigh, C. S. R., Corp, L. A., Ott, L. E., Chavez, S., & Morton, D. C. (2021). Storm surge and ponding explain mangrove dieback in southwest Florida following Hurricane Irma. *Nature Communications*, *12*(1), 4003. <https://doi.org/10.1038/s41467-021-24253-y>
- Lapointe, B. E., Barile, P. J., & Matzie, W. R. (2004). Anthropogenic nutrient enrichment of seagrass and coral reef communities in the Lower Florida Keys: discrimination of local versus regional nitrogen sources. *Journal of Experimental Marine Biology and Ecology*, *308*(1), 23–58. <https://doi.org/10.1016/j.jembe.2004.01.019>

- Lee, T., Johns, E., Melo, N., Smith, R., Ortner, P., & Smith, D. (2006). On Florida Bay hypersalinity and water exchange. *Bulletin of Marine Science*, 79, 301–327.
- Lopez-Rivas, J. D., & Cardenas, J.-C. (2024). What is the economic value of coastal and marine ecosystem services? A systematic literature review. *Marine Policy*, 161, 106033. <https://doi.org/10.1016/j.marpol.2024.106033>
- Manheim, F. T., Krantz, D. E., & Bratton, J. F. (2004). Studying Ground Water Under Delmarva Coastal Bays Using Electrical Resistivity. *Groundwater*, 42(7), 1052–1068. <https://doi.org/10.1111/j.1745-6584.2004.tb02643.x>
- Marshall, F. E., & Wingard, G. L. (2012). Florida Bay Salinity and Everglades Wetlands Hydrology circa 1900 CE: A Compilation of Paleoecology-Based Statistical Modeling Analyses. <https://pubs.usgs.gov/of/2012/1054/>
- Michael, H. A., Mulligan, A. E., & Harvey, C. F. (2005). Seasonal oscillations in water exchange between aquifers and the coastal ocean. *Nature*, 436(7054), 1145–1148. <https://doi.org/10.1038/nature03935>
- Moore, W. S. (1999). The subterranean estuary: a reaction zone of ground water and sea water. *Marine Chemistry*, 65(1–2), 111–125. [https://doi.org/10.1016/S0304-4203\(99\)00014-6](https://doi.org/10.1016/S0304-4203(99)00014-6)
- Moore, W. S. (2003). Sources and fluxes of submarine groundwater discharge delineated by radium isotopes. *Biogeochemistry*, 66(1), 75–93. <https://doi.org/10.1023/B: BIOG.0000006065.77764.a0>
- Moore, W. S. (2010). The Effect of Submarine Groundwater Discharge on the Ocean. *Annual Review of Marine Science*, 2(1), 59–88. <https://doi.org/10.1146/annurev-marine-120308-081019>

- Morra, G. (2018). Visualization. In G. Morra (Ed.), *Pythonic Geodynamics: Implementations for Fast Computing* (pp. 15–33). Springer International Publishing.
https://doi.org/10.1007/978-3-319-55682-6_2
- Murray, James. B., Wingard, G. L., Cronin, T. M., Orem, W. H., Wilard, D. A., Holmes, C. W., Reich, C., Shinn, E., Marot, M., Lerch, T., Trappe, C., & Landacre, B. (2010). *Evidence of Environmental Change in Rankin Basin, Central Florida Bay, Everglades National Park* (U.S. Geological Survey Open File Report 2010-1125).
<https://pubs.usgs.gov/of/2010/1125/ofr20101125.pdf>
- National Oceanographic and Atmospheric Administration. (2022). *Climate*.
<https://www.weather.gov/wrh/Climate?wfo=mfl>
- National Oceanic and Atmospheric Administration. (2023a). *Sea Water | National Oceanic and Atmospheric Administration*. <https://www.noaa.gov/jetstream/ocean/sea-water>
- National Oceanographic and Atmospheric Administration. (2023b). *Climate Page for South Florida*. <https://www.weather.gov/mfl/winteroutlookforsouthflorida>
- National Oceanic and Atmospheric Administration. (2024). *What percentage of the American population lives near the coast?*
<https://oceanservice.noaa.gov/facts/population.html>
- National Park Service. (2016). *Comprehensive Everglades Restoration Plan (CERP) - Everglades National Park (U.S. National Park Service)*.
<https://www.nps.gov/ever/learn/nature/cerp.htm>
- National Weather Service. (n.d.). *Estimating Wind Speed and Sea State with Visual Clues*.
National Oceanic and Atmospheric Administration.
<https://www.weather.gov/media/pqr/beaufort/beaufort.pdf>

- Null, K. A., Dimova, N. T., Knee, K. L., Esser, B. K., Swarzenski, P. W., Singleton, M. J., Stacey, M., & Paytan, A. (2012). Submarine Groundwater Discharge-Derived Nutrient Loads to San Francisco Bay: Implications to Future Ecosystem Changes. *Estuaries and Coasts*, 35(5), 1299–1315. <https://doi.org/10.1007/s12237-012-9526-7>
- Nuttle, W. K., Fourqurean, J. W., Cosby, B. J., Zieman, J. C., & Robblee, M. B. (2000). Influence of net freshwater supply on salinity in Florida Bay. *Water Resources Research*, 36(7), 1805–1822. <https://doi.org/10.1029/1999WR900352>
- Nyquist, J. E., Heaney, M. J., & Toran, L. (2009). Characterizing lakebed seepage and geologic heterogeneity using resistivity imaging and temperature measurements. *Near Surface Geophysics*, 7(5–6), 487–498. <https://doi.org/10.3997/1873-0604.2009022>
- Oehler, T., Bakti, H., Lubis, R. F., Purwoarminta, A., Delinom, R., & Moosdorf, N. (2019). Nutrient dynamics in submarine groundwater discharge through a coral reef (western Lombok, Indonesia). *Limnology and Oceanography*, 64(6), 2646–2661. <https://doi.org/10.1002/lno.11240>
- Orem, W. H., Holmes, C. W., Kendall, C., Lerch, H. E., Bates, A. L., Silva, S. R., Boylan, A., Corum, M., Marot, M., & Hedgman, C. (1999). Geochemistry of Florida Bay Sediments: Nutrient History at Five Sites in Eastern and Central Florida Bay. *Journal of Coastal Research*, 15(4), 1055–1071. <https://www.jstor.org/stable/4299024>
- Paepen, M., Hanssens, D., De Smedt, P., Walraevens, K., & Hermans, T. (2020). Combining resistivity and frequency domain electromagnetic methods to investigate submarine groundwater discharge in the littoral zone. *Hydrology and*

Earth System Sciences, 24(7), 3539–3555. <https://doi.org/10.5194/hess-24-3539-2020>

Price, R. M., Nuttle, W. K., Cosby, B. J., & Swart, P. K. (2007). Variation and uncertainty in evaporation from a subtropical estuary: Florida Bay. *Estuaries and Coasts*, 30(3), 497–506. <https://doi.org/10.1007/BF02819396>

Purkis, S. J., & Harris, P. (2017). Quantitative interrogation of a fossilized carbonate sand body – The Pleistocene Miami oolite of South Florida. *Sedimentology*, 64(5), 1439–1464. <https://doi.org/10.1111/sed.12367>

Reich, C. D., Shinn, E. A., Hickey, T. D., & Tihansky, A. B. (2002). Tidal and meteorological influences on shallow marine groundwater flow in the upper Florida Keys. 659–676. <https://pubs.usgs.gov/publication/70123291>

Robbins, B. (2023). Submerged Aquatic Vegetation Response to Submarine Groundwater Discharge. *Electronic Theses and Dissertations*. Georgia Southern University <https://digitalcommons.georgiasouthern.edu/etd/2634>

Robblee, M., Barber, T., Carlson, P., Durako, M., Fourqurean, J., Muehlstein, L., Porter, D., Yarbrow, L., Zieman, R., & Zieman, J. (1991). Mass mortality of the tropical seagrass *Thalassia testudinum* in Florida Bay (USA). *Marine Ecology Progress Series*, 71, 297–299. <https://doi.org/10.3354/meps071297>

Robert, T., Dassargues, A., Brouyère, S., Kaufmann, O., Hallet, V., & Nguyen, F. (2011). Assessing the contribution of electrical resistivity tomography (ERT) and self-potential (SP) methods for a water well drilling program in fractured/karstified limestones. *Journal of Applied Geophysics*, 75(1), 42–53. <https://doi.org/10.1016/j.jappgeo.2011.06.008>

- Rocha, C., Jiang, S., Ibánhez, J. S. P., Yang, Q., Mazi, K., & Koussis, A. D. (2022). The effects of subterranean estuary dynamics on nutrient resource ratio availability to microphytobenthos in a coastal lagoon. *Science of The Total Environment*, 851, 157522. <https://doi.org/10.1016/j.scitotenv.2022.157522>
- Rodemann, J. R., James, W. R., Santos, R. O., Furman, B. T., Fratto, Z. W., Bautista, V., Lara Hernandez, J., Viadero, N. M., Linenfelser, J. O., Lacy, L. A., Hall, M. O., Kelble, C. R., Kavanagh, C., & Rehage, J. S. (2021). Impact of Extreme Disturbances on Suspended Sediment in Western Florida Bay: Implications for Seagrass Resilience. *Frontiers in Marine Science*, 8, 633240. <https://doi.org/10.3389/fmars.2021.633240>
- Rucker, D. F., Noonan, G. E., & Greenwood, W. J. (2011). Electrical resistivity in support of geological mapping along the Panama Canal. *Engineering Geology*, 117(1–2), 121–133. <https://doi.org/10.1016/j.enggeo.2010.10.012>
- Samani, A. N., Farzin, M., Rahmati, O., Feiznia, S., Kazemi, G. A., Foody, G., & Melesse, A. M. (2021). Scrutinizing Relationships between Submarine Groundwater Discharge and Upstream Areas Using Thermal Remote Sensing: A Case Study in the Northern Persian Gulf. *Remote Sensing*, 13(3), 358. <https://doi.org/10.3390/rs13030358>
- Santos, I. R., Chen, X., Lecher, A. L., Sawyer, A. H., Moosdorf, N., Rodellas, V., Tamborski, J., Cho, H.-M., Dimova, N., Sugimoto, R., Bonaglia, S., Li, H., Hajati, M.-C., & Li, L. (2021). Submarine groundwater discharge impacts on coastal nutrient biogeochemistry. *Nature Reviews Earth & Environment*, 2(5), 307–323. <https://doi.org/10.1038/s43017-021-00152-0>

- Schulmeister, M. K., Butler, J. J., Healey, J. M., Zheng, L., Wysocki, D. A., & McCall, G. W. (2003). Direct-Push Electrical Conductivity Logging for High-Resolution Hydrostratigraphic Characterization. *Groundwater Monitoring & Remediation*, 23(3), 52–62. <https://doi.org/10.1111/j.1745-6592.2003.tb00683.x>
- Scott, T. M., Means, G. H., & Brewster-Wingard, G. L. (1997). Progress report on sediment analyses at selected faunal monitoring sites in north-central and northeastern Florida Bay (Report Nos. 97–534; Open-File Report). Florida Geological Survey.
- Shank, G. C., Evans, A., Yamashita, Y., & Jaffé, R. (2011). Solar radiation–enhanced dissolution of particulate organic matter from coastal marine sediments. *Limnology and Oceanography*, 56(2), 577–588. <https://doi.org/10.4319/lo.2011.56.2.0577>
- South Florida Water Management District. (2018). Sending Water South to Florida Bay South Florida Water Management District. <https://www.sfwmd.gov/our-work/florida-bay>
- Stabenau, E., Engel, V., Sadle, J., & Pearlstine, L. (2011). Sea-level rise: observations, impacts, and proactive measures in Everglades National Park. *Park Science*, 28(2), 26–30.
- Stabenau, E., & Kotun, K. (2012). *Salinity and Hydrology of Florida Bay Status and Trends 1990-2009* (South Florida Natural Resources Center Technical Series). National Park Service. <https://www.nps.gov/ever/learn/nature/upload/2012-1-FloridaBayComplete-508-2.pdf>
- Stainback, G. A., Lai, J. H., Pienaar, E. F., Adam, D. C., Wiederholt, R., & Vorseth, C. (2020). Public preferences for ecological indicators used in Everglades restoration. *PLOS ONE*, 15(6), e0234051. <https://doi.org/10.1371/journal.pone.0234051>

- Stieglitz, T., Rapaglia, J., & Bokuniewicz, H. (2008). Estimation of submarine groundwater discharge from bulk ground electrical conductivity measurements. *Journal of Geophysical Research: Oceans*, 113(C8), 2007JC004499. <https://doi.org/10.1029/2007JC004499>
- Sun, Z., Fan, Z., Zhu, C., Li, K., Sun, Z., Song, X., Xue, L., Liu, H., & Jia, Y. (2023). Study on the Relationship between Resistivity and the Physical Properties of Seafloor Sediments Based on the Deep Neural Learning Algorithm. *Journal of Marine Science and Engineering*, 11(5), 937. <https://doi.org/10.3390/jmse11050937>
- Swart, P. K., Berler, D., McNeill, D., Guzikowski, M., Harrison, S. A., & Dedick, E. (1989). Interstitial water geochemistry and carbonate diagenesis in the sub-surface of a Holocene mud Island in Florida Bay. *Bulletin of Marine Science*, 44(1), 490–514. <http://pascal-francis.inist.fr/vibad/index.php?action=getRecordDetail&idt=19735850>
- Swart, P. K., & Kramer, P. A. (2004). Geology of Mud Islands in Florida Bay. In *Developments in Sedimentology* (Vol. 54, pp. 249–274). Elsevier. [https://doi.org/10.1016/S0070-4571\(04\)80028-1](https://doi.org/10.1016/S0070-4571(04)80028-1)
- Swarzenski, P. W., Bratton, J. F., & Crusius, J. (2004). Submarine ground-water discharge and its role in coastal processes and ecosystems (Nos. 2004–1226). U.S. Geological Survey. <https://doi.org/10.3133/ofr20041226>
- Swarzenski, P. W., Reich, C., Kroeger, K. D., & Baskaran, M. (2007a). Ra and Rn isotopes as natural tracers of submarine groundwater discharge in Tampa Bay, Florida. *Marine Chemistry*, 104(1–2), 69–84. <https://doi.org/10.1016/j.marchem.2006.08.001>

- Swarzenski, P. W., Simonds, F. W., Paulson, A. J., Kruse, S., & Reich, C. (2007b). Geochemical and Geophysical Examination of Submarine Groundwater Discharge and Associated Nutrient Loading Estimates into Lynch Cove, Hood Canal, WA. *Environmental Science & Technology*, 41(20), 7022–7029. <https://doi.org/10.1021/es070881a>
- Swarzenski, P. W., & Izbicki, J. A. (2009). Coastal groundwater dynamics off Santa Barbara, California: Combining geochemical tracers, electromagnetic seepmeters, and electrical resistivity. *Estuarine, Coastal and Shelf Science*, 83(1), 77–89. <https://doi.org/10.1016/j.ecss.2009.03.027>
- Swarzenski, P. W., Reich, C., & Rudnick, D. (2009). Examining Submarine Ground-Water Discharge into Florida Bay by using ^{222}Rn and Continuous Resistivity Profiling (Nos. 2008–1342). U.S. Geological Survey. <https://doi.org/10.3133/ofr20081342>
- Szymczycha, B., Maciejewska, A., Winogradow, A., & Pempkowiak, J. (2014). Could submarine groundwater discharge be a significant carbon source to the southern Baltic Sea? *Oceanologia*, 56(2), 327–347. <https://doi.org/10.5697/oc.56-2.327>
- Tamborski, J. J., Rogers, A. D., Bokuniewicz, H. J., Cochran, J. K., & Young, C. R. (2015). Identification and quantification of diffuse fresh submarine groundwater discharge via airborne thermal infrared remote sensing. *Remote Sensing of Environment*, 171, 202–217. <https://doi.org/10.1016/j.rse.2015.10.010>
- Taniguchi, M., Burnett, W. C., Cable, J. E., & Turner, J. V. (2002). Investigation of submarine groundwater discharge. *Hydrological Processes*, 16(11), 2115–2129. <https://doi.org/10.1002/hyp.1145>
- Taniguchi, M., Dulai, H., Burnett, K. M., Santos, I. R., Sugimoto, R., Stieglitz, T., Kim, G., Moosdorf, N., & Burnett, W. C. (2019). Submarine Groundwater Discharge:

Updates on Its Measurement Techniques, Geophysical Drivers, Magnitudes, and Effects. *Frontiers in Environmental Science*, 7, 141.

<https://doi.org/10.3389/fenvs.2019.00141>

Tassy, A., Maxwell, M., Borgomano, J., Arfib, B., Fournier, F., Gilli, E., & Guglielmi, Y. (2014). Electrical resistivity tomography (ERT) of a coastal carbonate aquifer (Port-Miou, SE France). *Environmental Earth Sciences*, 71(2), 601–608.

<https://doi.org/10.1007/s12665-013-2802-4>

Thompson, S., Kulesa, B., & Luckman, A. (2012). Integrated electrical resistivity tomography (ERT) and self-potential (SP) techniques for assessing hydrological processes within glacial lake moraine dams. *Journal of Glaciology*, 58(211), 849–858. <https://doi.org/10.3189/2012JoG11J235>

Top, Z., Brand, L. E., Corbett, R. D., Burnett, W., & Chariton, J. (2001). Helium and Radon as Tracers of Groundwater Input into Florida Bay. *Journal of Coastal Research*, 17(4). <https://journals.flvc.org/jcr/article/view/81510>

United Nations Educational, Scientific and Cultural Organization. (2010). *World Heritage Committee inscribes Everglades National Park on List of World Heritage in Danger*. UNESCO World Heritage Centre. <https://whc.unesco.org/en/news/638/>

United Nations Educational, Scientific and Cultural Organization. (2018). *Everglades National Park*. UNESCO World Heritage Centre. <https://whc.unesco.org/en/list/76/>

Van Engelen, J., Oude Essink, G. H. P., Kooi, H., & Bierkens, M. F. P. (2018). On the origins of hypersaline groundwater in the Nile Delta aquifer. *Journal of Hydrology*, 560, 301–317. <https://doi.org/10.1016/j.jhydrol.2018.03.029>

Wanless, H. R., & Tagett, M. G. (1989). Origin, Growth and Evolution of Carbonate Mudbanks in Florida Bay. *Bulletin of Marine Science*, 44(1), 454–489.

- Williams, C. J., Jaffé, R., Anderson, W. T., & Jochem, F. J. (2009). Importance of seagrass as a carbon source for heterotrophic bacteria in a subtropical estuary (Florida Bay). *Estuarine, Coastal and Shelf Science*, 85(3), 507–514.
<https://doi.org/10.1016/j.ecss.2009.09.019>
- Wilson, A. M. (2005). Fresh and saline groundwater discharge to the ocean: A regional perspective. *Water Resources Research*, 41(2), 2004WR003399.
<https://doi.org/10.1029/2004WR003399>
- Wilson, J., & Rocha, C. (2012). Regional scale assessment of Submarine Groundwater Discharge in Ireland combining medium resolution satellite imagery and geochemical tracing techniques. *Remote Sensing of Environment*, 119, 21–34.
<https://doi.org/10.1016/j.rse.2011.11.018>
- Wu, Z., Zhu, H., Tang, D., Wang, Y., Zidan, A., & Cui, Z. (2021). Submarine groundwater discharge as a significant export of dissolved inorganic carbon from a mangrove tidal creek to Qinglan Bay (Hainan Island, China). *Continental Shelf Research*, 223, 104451. <https://doi.org/10.1016/j.csr.2021.104451>
- Yates, K. K., & Halley, R. B. (2006). Diurnal variation in rates of calcification and carbonate sediment dissolution in Florida Bay. *Estuaries and Coasts*, 29(1), 24–39.
<https://doi.org/10.1007/BF02784696>
- Zamrsky, D., Karssenbergh, M. E., Cohen, K. M., Bierkens, M. F. P., & Oude Essink, G. H. P. (2020). Geological Heterogeneity of Coastal Unconsolidated Groundwater Systems Worldwide and Its Influence on Offshore Fresh Groundwater Occurrence. *Frontiers in Earth Science*, 7, 339. <https://doi.org/10.3389/feart.2019.00339>

Zamrsky, D., Oude Essink, G. H. P., & Bierkens, M. F. P. (2024). Global Impact of Sea Level Rise on Coastal Fresh Groundwater Resources. *Earth's Future*, 12(1), e2023EF003581. <https://doi.org/10.1029/2023EF003581>

Zhang, Y., Li, H., Xiao, K., Wang, X., Lu, X., Zhang, M., An, A., Qu, W., Wan, L., Zheng, C., Wang, X., & Jiang, X. (2017). Improving Estimation of Submarine Groundwater Discharge Using Radium and Radon Tracers: Application in Jiaozhou Bay, China. *Journal of Geophysical Research: Oceans*, 122(10), 8263–8277. <https://doi.org/10.1002/2017JC013237>

Zieman, J. C., Fourqurean, J. W., & Frankovich, T. A. (1999). Seagrass die-off in Florida Bay: Long-term trends in abundance and growth of turtle grass, *Thalassia testudinum*. *Estuaries*, 22(2), 460–470. <https://doi.org/10.2307/1353211>

Zieman, J., Fourqurean, J. W., & Iverson, R. L. (1989). Distribution, Abundance and Productivity of Seagrasses and Macroalgae in Florida Bay. *Bulletin of Marine Science*, 44(1), 292–311.

APPENDICES

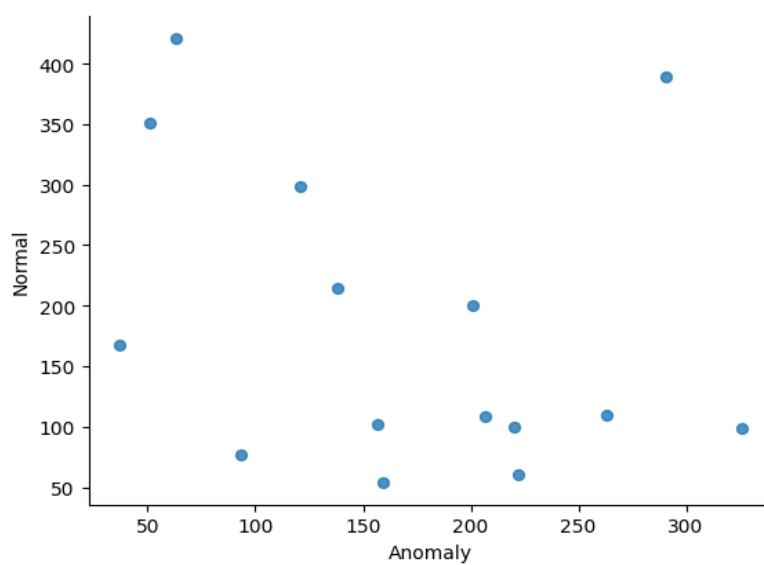


Fig. A.1: Scatter plot of aggregated radon activity for “A” and “N” zones of the three basins.

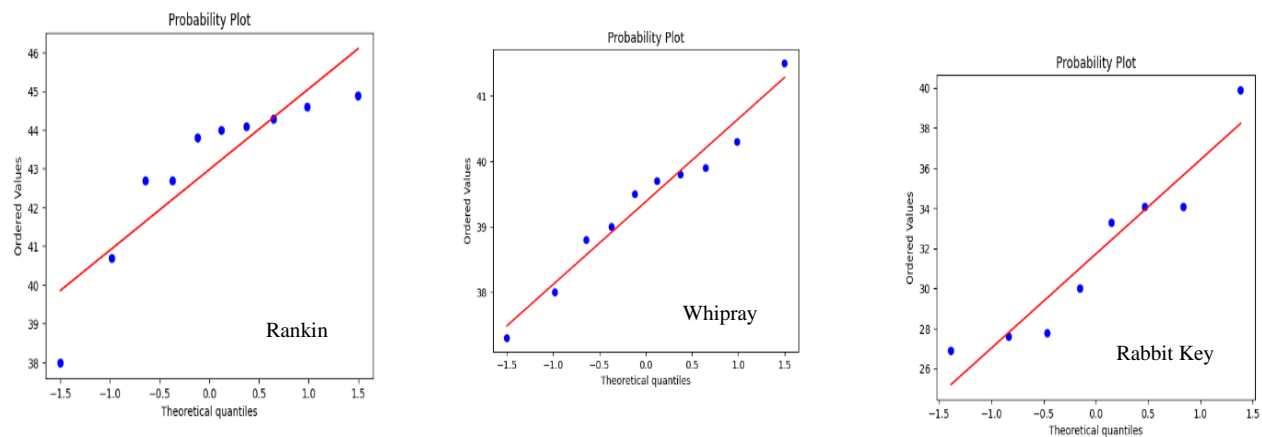


Fig. A.2: Probability plots of salinity measurements for the “A” and “N.”

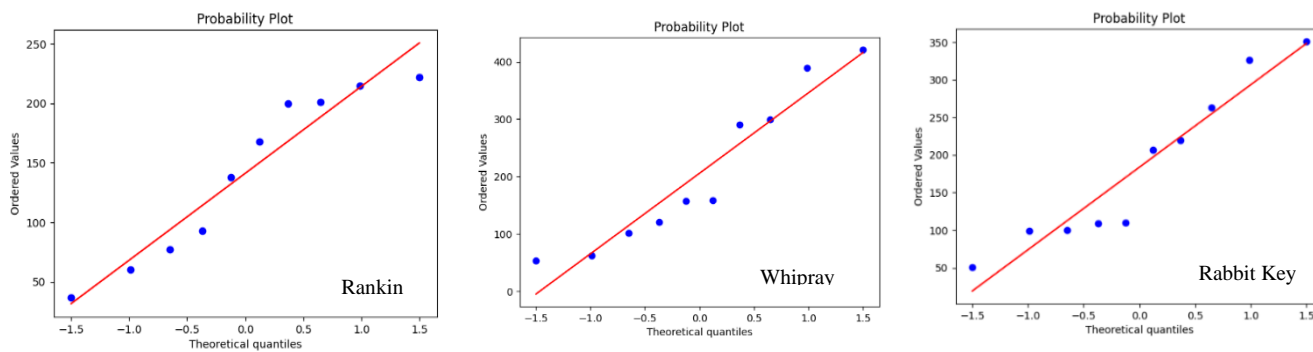


Fig. A.3: Probability plots of radon activity for the “A” and “N”.